Characterization of Steel Corrosion Products in Reinforced Concrete

by

INEKU AMHAYESUS METAFERIA

Under the supervision of

Dr. Beatriz Martín-Pérez

Co-supervisor

Dr. Reza Foruzanmehr

Thesis submitted to the University of Ottawa in partial fulfilment of the requirements of the degree of

Master of Applied Science in Civil Engineering

Department of Civil Engineering
Faculty of Engineering
University of Ottawa

Abstract

Steel corrosion is one of the major distress mechanisms that causes the deterioration of reinforced concrete structures around the world. It is an electrochemical reaction between the reinforcing steel and the surrounding concrete that produces a mass loss of the metal. Through the process of corrosion in reinforced concrete, iron ions get oxidized to form corrosion products (CP). Although multiple experiments and studies have been developed to understand the rheological behavior of corrosion products, this topic stays inconclusive. This work aims to characterize corrosion products at micro-scale in order to trace the progress of the formation of rust, to determine its nature and to analyse its rheological behavior in reinforced concrete. An experimental procedure to produce CP in the laboratory is also presented in this research. In addition, material characterization methods have been used to identify the iron oxide phases present in CP, determine their viscosity and rheological behavior and to study how CP flows in a porous media. In order to identify the different stages in the corrosion process, the CP was analysed at 2, 4, 6 and 8 weeks. The experiments identified four phases of iron oxide for each period. Furthermore, it was found that CP behaves as a shear-thinning slurry and as a result, its viscosity decreases with the applied shear rate. In addition, the damage caused by CP on concrete depends on the w/c ratio of the concrete mix and the exposure time to a corroding environment. The rebar mass loss results show that CP is formed in layers around the rebar, and the flow of each CP layer can differ.

Keywords: Corrosion products, iron oxide, rheological behavior, steel reinforcement, accelerated corrosion, corrosion-induced cracks.

Table of Contents

List of Figures

List of Tables

Nomenclature

CP: corrosion products

RC: reinforced concrete

FE: finite element

FEM: finite element model

SEM: scanning electron microscopy

XRD: x-ray diffraction

FTIR: Fourier transform infrared spectrometer

EDX: energy dispersive x-ray

R_v: Expansion coefficient

Acknowledgements

Foremost, I would like to express my warmest gratitude to my supervisors Dr. Martín-Perez and Dr. Foruzanmehr for the immense wealth of knowledge they shared throughout this valuable learning experience. Their guidance, patience compassion and motivation have been my fuel during the hard and easy times. I could not have been paired with better supervisors.

I would also like to acknowledge all the laboratory staff in the Civil and Mechanical Engineering Departments, mainly Dr. Muslim Majeed, Patrick D'Aoust and Luc Cloutier for their recommendations and patience.

Last but not least, a special thanks to my family and friends; I will forever be grateful to my parents, Yewubdar and Amhayesus for cheering me and being there for me, enduring all the long phone calls. My siblings Gohe, Metaferia and Abeba who never ceased to encourage and support me through many sleepless nights.

Chapter 1

1. Introduction

1.1 General

Nowadays, reinforced concrete (RC) is the most used construction material in the world. RC is a composite material that offers advantages such as its mechanical strength, resistance to fire, earthquake and weather, low maintenance cost, durability and formability (Song *et al.* 2007). However, steel reinforcement is prone to corrosion under specific conditions, becoming the most common deterioration mechanism in RC and impairing 55% of RC structures in Europe as stated by (Tilly 2007). Corrosion is an electrochemical phenomenon initiated when the concrete cover has a sufficient amount of chloride ions or is carbonated (Neville 1995). In cold countries such as Canada, the abundant use of de-icing salts (6 to 9 million tons of road salts per year) aggravates the impact of reinforcement corrosion process in RC structures (Canada. Environment Canada. 2012).

The Champlain Bridge in Montreal (Figure 1. 1), built 63 years ago is now obsolete due to severe damages on the concrete structure. Corrosion was found to be one of the main distress mechanisms that caused the deterioration of the reinforced concrete bridge (COWI 2017). As seen in Figure 1. 2, there were visible signs of corrosion all around the prestressing tendons and spalling of the concrete cover.

Figure 1. 1- Former Champlain Bridge, Montreal, QC (COWI 2017)

Figure 1. 2- Signs of corrosion in Champlain Bridge (COWI 2017)

The damage caused by corrosion is often unveiled by rust staining of the surface, cracking and spalling of the concrete cover and eventually by significant decrease of the structure's mechanical strength. This affects the serviceability and safety of RC structures. Fortunately, the structural deterioration caused by corrosion is slow.

Many studies have been completed to understand the nature of rust and how it behaves in RC (Suda *et al.* 1993; Ouglova *et al.* 2006; Andrade 2013). Researchers have conducted accelerated corrosion experiments on RC specimens; however, since corrosion is a time-consuming process, it is challenging to reproduce corrosion and the ensuing damage in a laboratory. In an effort to better study and foresee the effect of corrosion on concrete structures, researchers have attempted

to model this mechanism through analytical or FE modelling. A very common modelling strategy has been the thick-wall cylinder analogy, by assuming the concrete cover as a thick- wall cylinder pressurised by the accumulation of rust around the reinforcing steel. Some models have idealized the concrete cover as an elastoplastic material (Molina *et al.* 1993; Balafas *et al.* 2011), while others have used analytical models considering the corrosion products' compressibility and diffusion into cracks (Roshan 2017). However, some of these modelling assumptions have not been fully tested experimentally.

Despite the several findings around this topic, more research must be undertaken to further expand the knowledge on the distribution and migration corrosion products, and the effect of their rheological and mechanical properties on corrosion-induced concrete cracking. The studies must be able to recreate experimental corrosion products that can be representative of real reinforcing steel rust, to determine their nature and investigate their behavior in RC.

1.2 Objectives and Scope of the Study

Many researchers have tried to define the nature of corrosion products based on assumptions. However, since the assumptions have not been fully supported by experimental research, different studies reached have different conclusions. Hence there is a need for broader and more thorough analysis of the properties of corrosion products. It is also necessary to investigate how corrosion products migrate from steel reinforcement into the concrete. This thesis aims to address these issues by analyzing the characteristics of corrosion products and relating them to their behavior in RC. The main objectives of this work are listed below:

1. Prepare a realistic and time-considerate experimental protocol for the production of corrosion products representative of rust in RC.
2. Use different material characterization methods to characterize the rheological properties of corrosion products.
3. Prepare a realistic experimental protocol to create accelerated corrosion on steel reinforced cement paste samples.
4. Determine the permeation characteristics of corrosion products within cement pastes with different water-to-cement ratios.
5. Associate corrosion products' characteristics with their behavior in RC in different cement paste microstructures.

1.3 Organization of the Thesis

This thesis consists of 5 chapters including this one. Chapter 3 and 4 are written in a journal paper format. The details of each chapter are listed below.

- Chapter 1 presents a general introduction to the research's motivation as well as the objectives and scope of the work.
- Chapter 2 discusses the state-of-the-art in the literature in the form of a literature review. It first covers a brief introduction on the corrosion process and the electrochemical reactions associated with it. The types of corrosion products are then discussed. This chapter also presents a summary of research conducted on the nature and rheological behavior of corrosion products in reinforced concrete. Finally, the effect of corrosion products on concrete is reviewed.
- Chapter 3 provides an experimental protocol to produce corrosion products using an accelerated corrosion regime. In this paper, the corrosion products obtained are characterized. The second part of this chapter examines the rheological properties of corrosion products using SEM, XRD, EDS, rheometer, pycnometer, particle size analyzer and viscometer.
- In chapter 4, an experimental protocol in which reinforced cement paste samples are corroded is provided. Corrosion-induced damage in the cement paste during accelerated corrosion is documented and characterized. The results obtained are discussed to understand the distribution and migration of corrosion products in concrete.
- Chapter 5 summarizes the main results and findings of Chapters 3 and 4. In this chapter, a detailed list of lessons learnt during this study is also given, as well as ideas for future work to further the investigation.
- Finally, the complete experimental data and results are presented in the Appendices.

Chapter 2

2. Literature Review

2.1 Corrosion Process

2.1.1 Definition

Corrosion of reinforced concrete (RC) is a generally well understood phenomenon. As defined by ASTM International G15-02, corrosion is “the chemical or electrochemical reaction between a material, usually a metal, and its environment that produces a deterioration of the material and its properties”(ASTM international G15 -08 2008). Although corrosion is a spontaneous phenomenon, it generally takes place under the conditions in which concrete permeability is high, and thus steel reinforcement becomes exposed to the corroding environment. Rust is an expansive product formed by the oxidation of iron or a ferrous alloy (e.g., reinforcing steel bars), causing a reduction in the cross-section of the reinforcement, and internal tensile stresses and cracking in the concrete cover. As the cross-section of the steel reinforcements reduces, the capacity of the concrete member is compromised (ACI Committee 201 2008).

There are 2 mechanisms that induce reinforcement corrosion in RC: one induced by chloride ions and one initiated by concrete carbonation (ACI Committee 201 2008). In cold-weather countries, RC is exposed to chloride ions through de-icing salts used in the winter, making chloride-induced corrosion more prevalent in Canada. In the presence of moisture (H_2O) and oxygen (O_2), bare steel is prone to corrosion. When iron (Fe) comes in contact with chloride ions (Cl^-) in an oxidizing and moist environment, electrochemical reactions take place spontaneously. However, when steel is embedded in concrete, such as in reinforced concrete, it is protected from the outside environment by the alkalinity of the concrete. Concrete is known to have a high pH of around 13.5 (Bertolini 2008). As the process of corrosion process takes several years, it passes through two main stages

called initiation and propagation, before reaching the end of service life. Figure 2. 1 shows the time for the service life of RC where the two stages of corrosion are included.

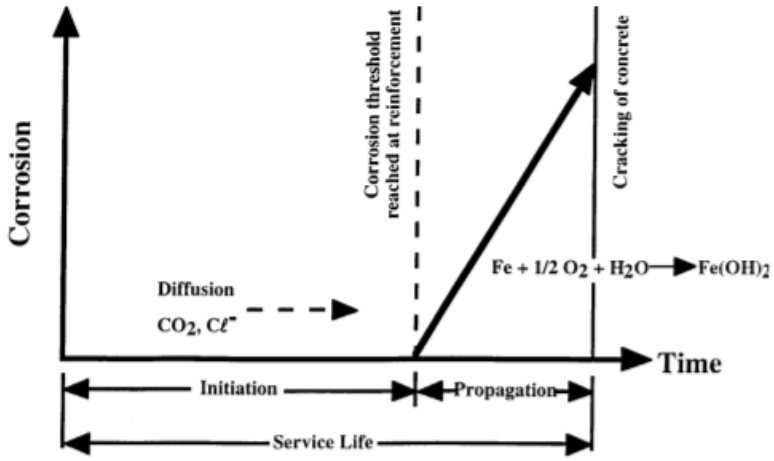

Figure 2. 1- Service life of concrete exposed to corrosion (Tuutti 1982)

In the presence of oxygen (O_2), the high pH environment of the concrete cover forms a thin film layer around the reinforcement. This layer is known as "the passive layer". Under normal environmental conditions, the layer protects the metal from corroding by slowing down the electrochemical reactions between the reinforcing bars and the surrounding environment, and the metal is passivated (Tuutti 1982). During the initiation stage, if sufficient amounts of chloride ions (Cl^-) and/or carbon dioxide (CO_2) from the atmosphere penetrate the concrete cover reaching the reinforcement layer, the passive layer protecting the reinforcement from corroding is impaired, depassivating the embedded steel and triggering the corrosion process. This is followed by the propagation stage, during which corrosion proceeds and by-products called rust are formed through the oxidation of steel and reduction of oxygen (Pacheco *et al.* 2012). Rust is known to have a relatively low density (3,970 kg/m^3 – 4,345 kg/m^3) in comparison to the original reinforcing steel (7,850 kg/m^3- 8,050 kg/m^3) (Ouglova *et al.* 2006). As a result, the surrounding concrete is subject to tensile stresses instigated by the expansive formed products. When the tensile stresses induced by this pressure exceed the tensile capacity of the concrete cover, cracking occurs. Finally, the mechanical strength of the RC element is compromised when major cracks are formed and spalling/and or delamination of the concrete cover takes place.

Carbonation-induced corrosion mostly occurs in urban and industrialized areas. Carbonation is a process by which carbon dioxide from air penetrates into the concrete and reacts with calcium hydroxide to form calcium carbonate. Due to the reduction of alkalinity in the concrete, the pH of the concrete pore solution in the hardened cement paste reduces to a value of approximately 9. At a pH lower than 9, corrosion can be triggered and the protective layer on the reinforcement gets destroyed. Moreover, corrosion may be initiated because of the presence of other distress mechanisms causing cracks and creating access of CO_2 to the steel reinforcement, thus accelerating the damage. Steel corrosion can be evaluated through several tools which can determine the likelihood of reinforcement corrosion present in the concrete, as well as the corrosion rate (ACI Committee 201 2016).

2.1.2 Initiation Stage

Corrosion process is triggered when chloride ions (or CO_2 molecules) travel from the outside environment to the passive layer through the concrete cover. This process is affected by several factors such as the thickness of the concrete cover. Regulations regarding concrete covers are presented in CSA A23.1-14 Table 17. Depending on the type of structure and environmental surroundings, specific concrete cover dimensions must be adopted (CSA A23.1-14 2014). In addition to this, the permeability of the concrete, the water-to-cement ratio, the alkalinity and the amount of chloride ions present are aspects that can influence the timing, type and result of the corrosion process.

In general, it is believed that the chloride corrosion threshold, above which corrosion is initiated, is attained when 0.15% to 0.30% water-soluble chloride by mass of cement reach the reinforcement layer; at this point the protective layer is depassivated and the propagation stage begins (Kosmatka *et al. 2002;* Trejo et *al. 2019).*

2.1.3 Propagation Stage

The propagation stage begins when electrochemical reactions take place between the steel bars and the pore solution of the concrete cover and chloride ions. The protected areas of the bars act as cathodes and the unprotected areas act as anodes. The anodic reaction takes place when the iron in the steel bars is oxidized releasing iron ions and electrons.

$$Fe \rightarrow Fe^{++} + 2e^{-} \qquad Eq\ 2.1$$

When it comes to the cathodic reaction, water, oxygen and electrons come in contact to form hydroxyl ions.

$$2H_2O + O_2 + 4e^- \rightarrow 4(OH)^- \qquad Eq\ 2.\ 2$$

Following these two reactions, oxygen reacts with the produced ferrous irons and hydroxyl ions to form corrosion products (ACI Committee 201 2008).

Because the reaction is separated into cathodic and anodic reactions, the corrosion is most likely a localized corrosion. This can also be explained by the fact that the amount of moisture, oxygen and chloride ions are not uniform along the reinforcing bars (Bertolini 2008). As seen in Figure 2. 2 and Figure 2. 3, the intensity of corrosion and the formation of CP is localized along the length of a steel rebar and around its perimeter, respectively (Qiao *et al.* 2016).

Nevertheless, most experimental studies and models are based on the assumption that CP is uniformly and smoothly distributed along the reinforcing bars, to simplify the phenomenon (Molina *et al.* 1993; Balafas *et al.* 2011).

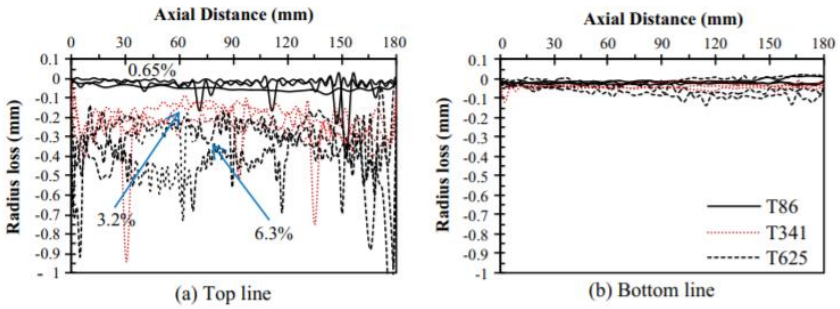

Figure 2. 2- Distribution of rust along the length of a steel bar in RC: (a) Top line (b) Bottom line (Qiao *et al.* 2016)

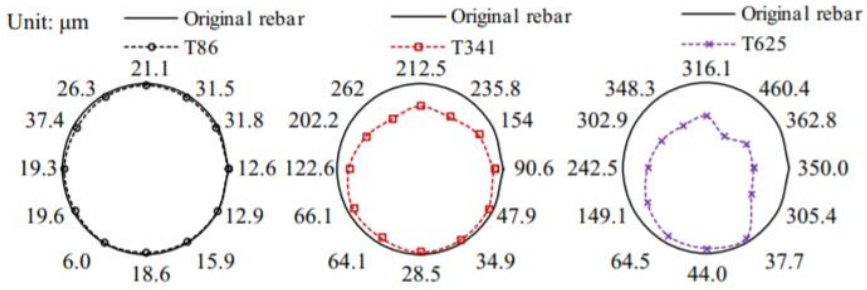

Figure 2. 3- Distribution of rust around the circumference of a steel bar in RC (Qiao *et al.* 2016)

As CP accumulates around the reinforcing bars, tensile hoop stresses are created all around the concrete cover. When these tensile stresses attain the maximum tensile strength of the concrete, cracks are formed. During this stage, the mechanical properties, durability and integrity of the concrete are highly affected when the steel bars' cross-sections are reduced and cracks are initiated (Pacheco *et al.* 2012). The concrete quality, the environmental conditions and the concrete cover depth are known to have a relatively big impact on this phase. They can control the rate of corrosion as well as the propagation of cracks in the concrete cover.

Researchers have also observed that the type of expansive corrosion products affects the concrete in different ways (Jaffer *et al.* 2009). According to Gotić *et al.*, dried samples of corrosion products can be formed in different iron oxide phases. Each phase has its own chemical and rheological properties. One of the main differences between the phases is their unit volume with an increase of up to six times the volume of the parent iron (see Figure 2. 4). Hence, the flow of corrosion products in the concrete is correspondingly different and in consequence the durability of the concrete can be affected to deferent degrees. The main identified iron oxide phases are: magnetite, goethite and lepidocrocite (Gotić *et al.* 2007).

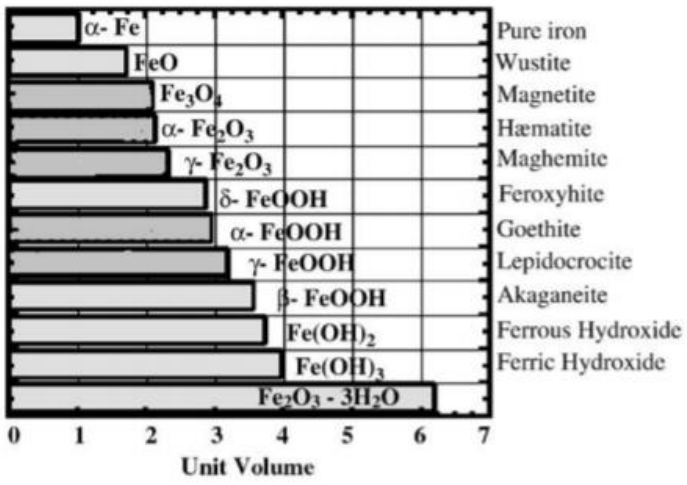

Figure 2. 4- Expansive character of iron oxide phases (Jaffer *et al.* 2009)

Concrete being a porous media allows the permeation and movement of materials such as corrosion by-products within the concrete. However, the permeation is controlled by various factors. The water-to-cement ratio (w/c) of a concrete mix plays a big role as it is directly related to the concrete matrix's porosity and permeability. According to the Canadian Standard Association (CSA A23.1-14/A23.1-14), the w/c for an RC mix should not be lower than 0.4 for

structural concrete exposed to aggressive environments (i.e., C1 exposure class) (CSA A23.1-14 2014). The initial porosity of concrete (even before being exposed to aggressive media) increases when the w/c increases, and vice versa. In porous media such as that made of cementitious materials, the capillary pores are almost twice as much as the gel pores. For a high w/c ratio, these capillary pores are connected, and the water transport is governed by the interconnectedness of the capillary porosity. For this reason, the permeability of the cement paste is higher. On the other hand, when the w/c is low, the gel pores will contribute to the water penetration in the concrete matrix. According to Powers et *al.*, the minimum capillary permeability of concrete is called the depercolation threshold (Powers et *al.* 1954; Powers et *al.* 1970).

Along with the w/c ratio, the corrosion rate is one major factor that governs the propagation stage of the corrosion process. As defined by Andrade and Alonso (2001), the corrosion rate is the amount of metal oxidized per unit of metallic surface over a certain period of time. It is generally used to determine the development of corrosion and to predict the service life of an RC structure. The propagation stage and more specifically the corrosion rate is usually influenced by the availability of oxygen (O_2), the ratio of the cathode-to-anodes areas and the electrical resistivity in the concrete (ACI Committee 201 2008).

2.2 Reinforcing Steel Corrosion Products

2.2.1 Production of Corrosion Products

Corrosion is a lengthy naturally occurring process. Therefore, accelerated corrosion tests are used to predict the corrosion behavior of steel reinforcement. Throughout the years, different researchers have proposed and used different methods of production of corrosion products, each trying to represent CP as realistic as possible.

Suda *et al.* (1993) conducted an experimental program to produce and study corrosion products. The research focused on chloride-induced reinforcement corrosion. With the incentive to do a nonlinear FE (finite element) analysis of corrosion-induced cracking, they created concrete samples with deformed steel bars. After curing the specimens in the laboratory for 4 weeks, they were transported to the exposure site where oxygen (O_2), water (H_2O) and chloride ions (Cl^-) had easy access through the concrete cover to reach the bars. Following a period of 5-year exposure,

the specimens were cut along the sections A-A and B-B in Figure 2. 5, and the corrosion products were then collected by scraping off the concrete cover and the corroded bars (Suda *et al.* 1993).

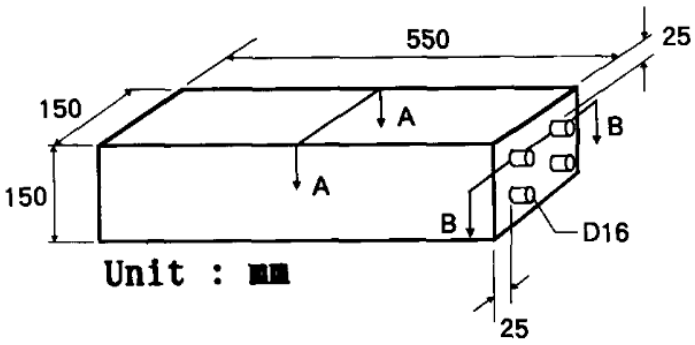

Figure 2. 5- Concrete sample used to collect corrosion products by Suda *et al.* (1993)

In 2005, Konopka used iron filling from a steel reinforcement bar to study corrosion products. The principle was based on introducing air bubbles through an acidic aqueous solution to accelerate the corrosion process of a steel rebar. The solution was able to transfer electric current through the bars, allowing cathodic and anodic reactions to occur. Once the corrosion products were collected in forms of flakes, they were then dried and tested (Konopka 2005) . Almost a decade later, Balafas and Burgoyne (2011) improved Konopka's experimental procedure by adding a concrete ring around the reinforcement bar to incorporate the effect of the concrete cover on the corrosion process.

Another approach followed by some researchers was the production of corrosion products from low-alloy steel samples (Ouglova *et al.* 2006). Low-alloy steel samples were plunged in an aerated solution containing 100 ppm of chloride ions. This solution also contained sodium hydroxide (NaOH) to regulate the pH level of the environment. This helped to simulate the real conditions of corrosion as it occurs in a high alkaline environment such as concrete. Two steel samples were prepared; one of them was dried in the oven at 50°C for 24 hours whereas the second sample was dried for 48 hours. By the end of the experiment, the corrosion products were obtained in powder form so that they could be characterized using material characterization methods (Ouglova *et al.* 2006).

In 2012, Zhao *et al.*, in an effort to produce corrosion products as similar as natural corrosion products, proposed a new method of production. This method proposes to use the rust produced on the surface of steel bars that are embedded in a concrete structural member. The structural

member (beam in this case) was collected from a building in Japan after 40 years of service. This beam came from a tidal zone with an average temperature of 26°C and 70% humidity. The flaky rust was peeled from the top and bottoms surfaces using coarse sandpapers (Figure 2. 6 (a)). As seen in Figure 2. 6 (b), the flakes were then grinded into fine particles and then sieved to be classified according to the different particle sizes (Zhao *et al*. 2012).

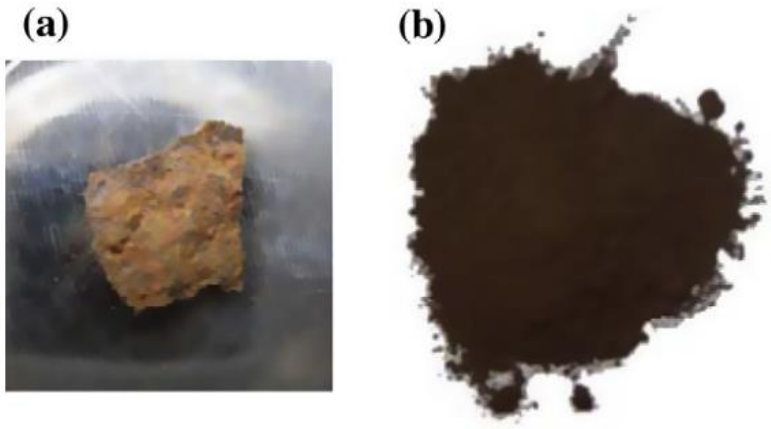

Figure 2. 6- (a) Flaky rust sample, (b) powder rust sample (reproduced from Zhao *et al.* (2012))

The same group of researchers conducted another study with a different approach (Zhao *et al.* 2012). The first method consisted of using an electrochemical current to accelerate the corrosion process. For this, a cylindrical concrete sample with a steel rebar inserted longitudinally is needed. The two ends of the bars are interconnected with wires and sealed with epoxy. A saline solution of 3.5% concentration is used as a water bath for the experimental setup. For 24 hours, the wires are connected to an electric current with a power density of 300 $\mu A/cm^2$. The second method used to generate corrosion products uses wet and dry cycles to accelerate the corrosion process. For this procedure, the pouring and curing of the reinforced concrete is done in an artificial climate laboratory. Every 3 days, for 4 hours, a 3.35% saline solution is sprayed on the concrete and the laboratory temperature is set to 40 °C to dry the samples. This process is repeated for 2 calendar years. For both methods, once the accelerated corrosion process is ended, the samples are cut and the corrosion products are collected (Zhao *et al.* 2012).

Andrade has proposed 2 types of laboratory procedures for the production of corrosion products through accelerated corrosion (Andrade 2013). The first test consists of putting a steel bar in an alkaline solution containing calcium hydroxide and sodium chloride. The corrosion products are developed all around where the rebar is submerged into the solution (Figure 2. 7). With the second

test, the corrosion products are generated in the hole of a cylindrical concrete sample where there is a steel bar. For 2 months the hole was sprayed with a solution containing sodium chloride and constantly being stirred. The bar is then connected to a stainless-steel mesh to complete an electric circuit (Figure 2. 8). The iron oxide produced is collected from the hole and dried at ambient temperature (Andrade 2013).

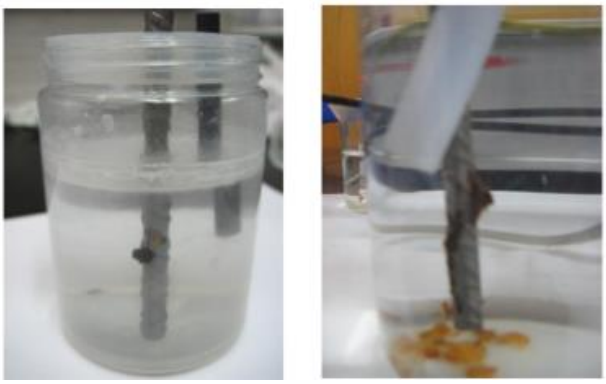

Figure 2. 7- Test 1 by Andrade (Andrade 2013)

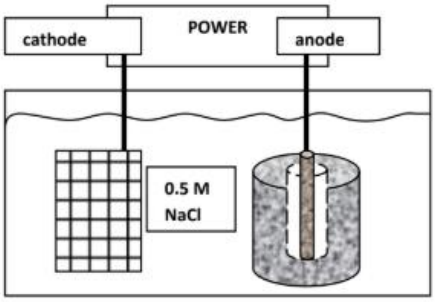

Figure 2. 8- Test 3 by Andrade (Andrade 2013)

2.2.2 Nature of Corrosion Products

The literature describing the nature of corrosion products resulting from steel reinforcement corrosion is very limited and mostly supported by assumptions. When it comes to the nature of corrosion products, numerous researchers have indicated different assumptions to base their work. These assumptions play a critical role when modelling the build-up of CP around the reinforcement steel and the ensuing concrete cover cracking. Even though researchers have proposed their assumptions, the nature of corrosion products has yet to be studied thoroughly with experimental tests.

Molina *et al.* (1993) was one of the first ones to model the mechanical nature of CP to simulate corrosion-induced cracking in the concrete cover using FE. They assumed that CP has the same properties as liquid water (i.e., bulk modulus of 2 GPa). Liquid water was said to be the main component of corrosion products and so, it was assumed that CP has the same rheological and mechanical properties. In the FEM (finite element model), they modelled the corrosion products in such a way that the mechanical properties (bulk modulus) change linearly as CP is transformed from iron to rust (Molina *et al.* 1993).

A few years later, a new assumption for the nature of CP was presented by Lundgren (2002), who assumed that the stiffness of corrosion products increases with the applied stress level. This is typical behavior of granular materials. This fact led Lundgren to believe that corrosion products can be assumed to behave similar to a granular material (Lundgren 2002).

Lundgren's assumption was supported by Oulgova *et al.* in 2006. In their thesis, they measured experimentally the strain versus stress in which they observed the presence of a hysteresis curve between the loading and unloading parts of the graph (Figure 2. 13). Based on their observations, they confirmed that corrosion products behave as a granular material. The mechanical properties of CP, including the Young's modulus was determined based on the same assumption (Ouglova *et al.* 2006).

Andrade, in a more recent study (Andrade 2013), has proved the assumption made in her previous work (Molina *et al.* 1993). After producing CP using her first method, she noticed that rust spots appear to be viscous. The author stated that by looking at the CP through a magnifying glass, they appear as "a flower having small petals containing water in between them". Furthermore, the author observed that if the water in the corrosion product is dried up, CP collapse and lose all their mechanical properties (Figure 2. 9). Hence the expansive character of corrosion products comes from its hydrophilic property, its ability to retain water molecules. For these reasons, Andrade (2013) validated the assumption that states that corrosion products have the same properties as a liquid, because they behave as a granular material in suspension and do not stay intact without the presence of water.

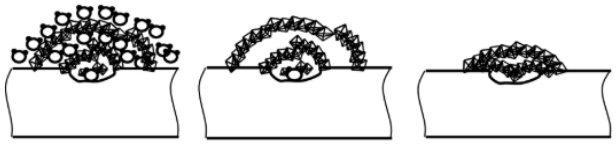

Figure 2. 9- Behavior of rust grains as water evaporates (Andrade 2013)

2.2.3 Types of Iron Oxides

The final by-product of steel corrosion, corrosion products, also known as rust, involves different compounds. Each compound exhibits unique chemical and physical properties. Most of them can be distinguished by their colors. Nevertheless, when they are not perceptible with their color, test such as XRD or Raman spectroscopy can be used to differentiate them. In order to understand the rheological behavior of CP in reinforced concrete, it is crucial to identify and study all the iron oxide phases created around reinforcing bars.

Oh *et al.* have identified nine different phases of oxides and oxyhydroxides that can be obtained from the corrosion process (Oh *et al.* 1998). These phases include: Goethite ($Fe_3O(OH)$), Magnetite (Fe_3O_4), Lepidocrocite (FeO(OH)), Hematite (Fe_2O_3), Maghemite (Fe_2O_3, γ-Fe_2O_3), Iron hydroxide (Fe(OH)2), Iron trihydride (FeH3), Akaganeite (FeO(OH) and Feroxyhyte (FeO(OH). The study of corrosion products and their phases is very recent, and thus the literature is limited in this area. One way to characterize each phase is by looking at their expandability (Figure 2. 4).The least and most expandable iron oxide phases in comparison to pure iron (Fe) are magnetite and akageneite) (Jaffer *et al.* 2009).

The literature shows that the formation of iron oxide phases depends on the nature of the corrosive environment. Nonetheless, it has been observed that the three most common phases reoccurring in reinforcement corrosion are magnetite, goethite and lepidocrocite (Antunes *et al.* 2003).

Gotić and Musić (2007) observed that the different phases of iron oxide were formed in different layers on the surface of the steel in RC before they start to diffuse through cracks and the concrete matrix. Magnetite was found on the layer adjacent to aggregates and hematite in the vicinity of the cement paste (Gotić and Musić 2007). This study contradicts one form 2003, wherein exposure times of 1, 2 and 3 months were used to study the formation of CP (Antunes *et al.* 2003). In this study, no layers of iron oxide phases were observed in the distribution of CP around a rebar and

lepidocrocite was identified. In conclusion, there are no apparent layers formed with time during the oxidation process (Antunes *et al.* 2003).

Antunes *et al.* (2003) also studied the iron oxide in CP in an attempt to define their morphology. Microscopic observation highlighted that lepidocrocite takes the form of crystalline globules or fine plates in some cases. Goethite has a globular structure (also known as cotton balls), and magnetite is represented by dark flat regions with circular disks (Antunes *et al.* 2003).

2.3 Properties of Corrosion Products

Multiple researchers have worked to determine the properties of corrosion products. Nevertheless, the literature around this topic is still very limited. Since the 1970's, various material characterization methods have been applied to determine the elemental, crystalline, rheological, physical and chemical properties of CP.

2.3.1 Elemental Properties

One of the characterization methods used to study the elemental properties of corrosion products is X-ray diffraction (XRD). Diffraction is a phenomenon that occurs when a beam of electromagnetic waves encounters an obstacle and the rays undergo a constructive or destructive interference (Robotti 2013). In a study by Suda *et al.* in 1993, rust was collected from corroded reinforcing bars to identify by XRD analysis the crystalline phase that exist in CP. The qualitative and quantitative XRD analysis of CP showed the presence of magnetite, goethite and lepidocrocite with a total volume percentage of 30%. The nature of each phase was described as "amorphous" and "disorganised" (Suda *et al.* 1993) . The same phases were also found dominant in CP in another study (Vera *et al.* 2009), wherein iron oxide from different environmental conditions (marine, industrial, polished steel, unpolished steel) was examined However, in this study the presence of akageneite was also detected specially in the areas where the chloride concentration was relatively high (Vera *et al.* 2009).

Table 2. 1- Percentage of phases characterized in different concretes (Aperador *et al.* 2011)

Concrete	Phase Characterized, %			
	Magnetite (Fe_3O_4)	Wuestite (FeO)	Goethite (a-FeOOH)	Iron
AASA	6.4	3.71	13.88	76.01
AASL	3.95	4.11	3.45	88.49
OPCA	5.75	2.31	7.72	84.22
OPCL	6.76	3.31	6.63	83.29

Aperador *et al.* (2011) used XRD to characterize the CP that was formed at the interface of steel and concrete. They found that the main CP components were magnetite, goethite and wuestite (FeO). The volume percentage for each phase was also quantified and presented in Table 2. 1 for concretes exposed to different exposure conditions: AASA/OPCA exposed to an accelerated carbonation chamber, and AASL/OPCL exposed to a laboratory environment with the accelerated chloride corrosion technique. In almost all scenarios, magnetite and goethite are the predominant components(Aperador *et al*. 2011).

In a more recent study (Zhang *et al.* 2019), XRD was used to determine the composition of CP under different current density levels during the accelerated corrosion process. As seen in Table 2. 2, the level of impressed current density increases, as the volume percentage of iron oxide increases. For the five iron oxide phases that were identified, it is possible to observe that the amount of magnetite and goethite increases when the current density increases, but the percentage of lepidocrocite decreases when the current density increases(Zhang *et al.* 2019).

Table 2. 2- Components of corrosion products with increasing current density (Zhang et *al.* 2019)

Impressed current density ($\mu A/cm^2$)	Mass fraction of different components (%)						Iron oxides (%)	Iron hydroxyl oxides (%)
	FeO	Fe_2O_3	Fe_3O_4	α-FeO(OH)	β-FeO(OH)	γ-FeO(OH)		
50	11.03	9.54	27.88	3.12	10.64	37.79	48.45	51.55
100	12.86	13.2	27.04	1.64	6.04	39.25	53.10	46.90
200	22.78	5.98	32.68	1.56	4.81	32.19	61.44	38.56
300	13.44	14.52	44.73	1.33	6.10	19.88	72.69	27.31
Nature sample	4.19	0.80	4.82	5.19	13.08	71.92	9.81	90.19

Another method that is used to identify properties of CP is Energy Dispersive X-ray (EDX). EDX is an analytical X-ray technique that is used for the elemental analysis of materials. The amount of each element in a specimen can be determined by detecting and identifying the characteristic X-rays. The EDX system can put the qualitative and quantitative analyses together to form a map of

the spatial variation of elements that exist in a specimen with their corresponding amounts. A study on the cross-section of a corroded reinforcing bar shows that the mill-scale (a thin layer of flaky iron oxide) is essentially composed of iron and oxygen (Gotić and Musić 2007). The EDS quantitative analysis is not completely accurate as lighter elements such as oxygen can be mistaken for other elements (Gotić and Musić 2007). In a similar study, Jaffer and Hansson (2009) determined the variation of iron to oxygen ratio of the mill scale with time. They concluded that a corroded bar has a lower Fe/O ratio than a corroding bar that is recently embedded into concrete (Jaffer and Hansson 2009).

Energy dispersive X-ray spectroscopy, EDX (or EDS), has also been used to determine the distribution of certain elements through the length and cross-section of a reinforced concrete sample that is undergoing corrosion. This can be used to follow the penetration of iron oxide products through concrete cracks. Zhao *et al.* (2012) showed the presence of Fe and O is high immediately adjacent to the rebar surface where corrosion's electrochemical reactions occur. However, there was no sign of iron or oxygen in the concrete cover cracks, which led to the conclusion that corrosion products do not penetrate through the cracks (Zhao *et al.* 2012).

2.3.2 Crystalline Properties

One other way to characterize CP is by identifying the morphology of its crystals. Scanning electron microscopy (SEM) is one of the methods that allows to do so. SEM produces images by scanning a sample with a high-energy electron beam. Each crystalline phase is associated with distinct morphology. The morphology of each phase is used to identify the types of material that exist in CP. SEM is also used to conduct particle size analysis in the case where the material is homogeneous, and the shapes are easily recognizable.

The literature (Gotić and Musić 2007) shows that cotton balls are typical representation of goethite (Figure 2. 10), sandy crystals can be associated with lepidocrocite (Figure 2. 11) and short rods with magnetite (Figure 2. 12). The results in both studies correlate well with the iron oxide phases that were identified with EDS and XRD (Gotić and Musić 2007; Ouglova *et al*. 2006).

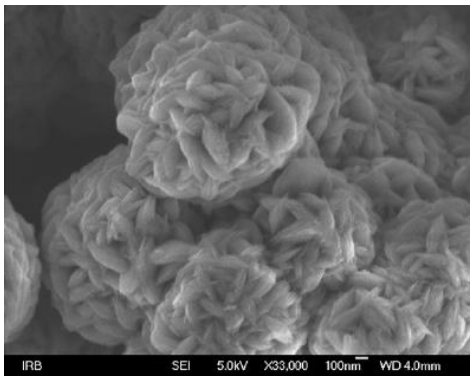

Figure 2. 10- SEM image of Goethite (Gotić and Musić 2007)

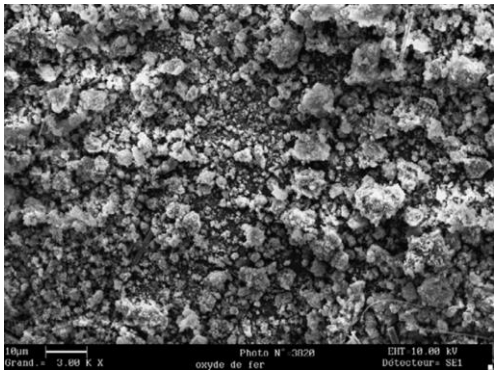

Figure 2. 11- SEM image of Lepidocrocite (Ouglova *et al.* 2006)

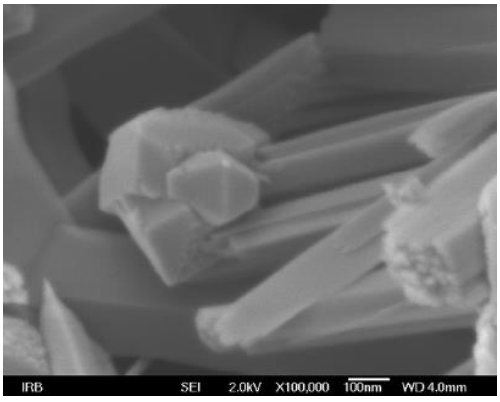

Figure 2. 12- SEM image of Magnetite (Gotić and Musić 2007)

2.3.3 Rheological Properties

Viscosity is a measure of a fluid's resistance to flow, it is "a quantity expressing the magnitude of internal friction, as measured by the force per unit area resisting a flow in which parallel layers unit distance apart have unit speed relative to one another" as defined by the Oxford English Dictionary. If a fluid is said to have a large viscosity, then it has a higher resistance to motion. On the other hand, one can say that a fluid with low viscosity flows. The viscosity of the flow is one of the main properties that is used to measure and characterize viscoelastic fluids. Viscosity is known to vary with temperature, the shear force applied to the fluid and the pressure in the fluid.

Rheology is the theory that deals with the deformation and flow of liquid materials, especially for non-Newtonian liquids and materials. Out of all the properties, the rheological behavior of corrosion product is the least studied up to date. This is due to the fact that most researchers assume that CP is an elastic material (liquid water or granular materials) (Molina *et al.* 1993; Lundgren and Gylltoft 2009; Ouglova *et al.* 2006)

In 2011 and 2012, two group of researchers reached different conclusions on whether or not CP move away from the reinforcement and penetrate the concrete matrix. Keivan and Hossein (2011) assumed that all the porous zone around the reinforcement should be filled before CP penetrates through the cracks (Liu and Weyers 1998). On the other hand, Zhao *et al*. (2012) found that the pores around the reinforcement are not necessarily all filled before CP starts to flow into cracks. This contradiction shows that it is important to understand the rheological behavior of CP(Zhao *et al.* 2012).

In their research, Ouglova *et al*. (2006) have examined how CP behaves under varying stress. The results show that the loading and unloading curves are not superimposed (Figure 2. 13). This proves that CP does not follow Newton's elastic relation; it behaves like non-Newtonian (visco-elastoplastic) materials (Ouglova *et al.* 2006).

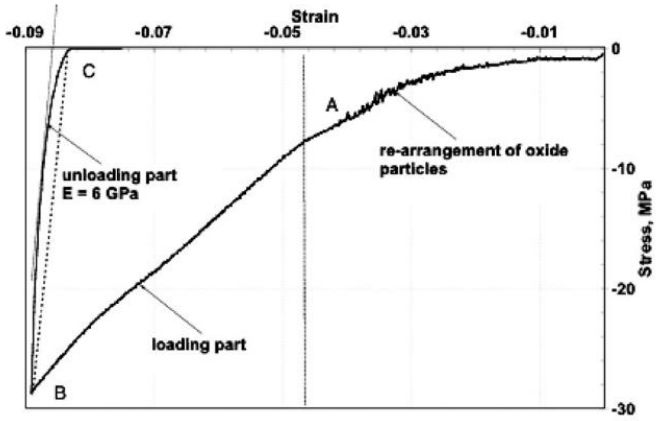

Figure 2. 13- Stress vs strain curve of iron oxide (Ouglova *et al.* 2006)

Non-Newtonian fluids or more specifically viscoelastic fluids are very complex in their nature of flow rheology and their interaction in a porous media. Non-Newtonian fluids can exhibit different types of behaviors when they are subjected to stress. As shown in Figure 2. 14 , non-Newtonian fluids can behave as Bingham plastic, dilatant, pseudoplastic with yield or pseudoplastic. Bingham plastics are classified as viscoelastic materials that flow as viscous fluid at high stresses but not at low stresses. Pseudoplastic can be used to characterize a non-Newtonian fluid that is shear-thinning. Finally, dilatant fluids are shear thickening (He *et al.* 2004)

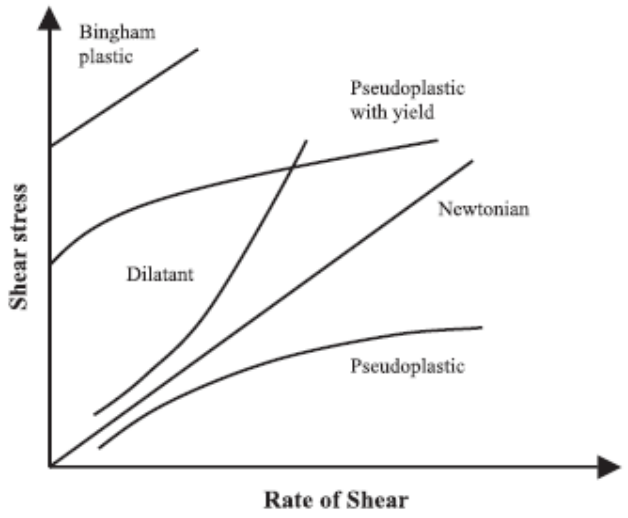

Figure 2. 14- Behavior of Non-Newtonian fluids under stress (He *et al.* 2004)

Multiple parameters have high impact on the rheological properties of slurries and colloidal solutions. The effect of particle concentration and particle size on the flow of these types of materials have been studied time after time. Leong *et al.* (1995), studied the effect of particle size

on colloidal zirconia (ZrO_2) rheology. Their study was based on the Van der Waals attraction (VDW) theory, which states that the attraction between two particles is stronger for larger particles. This attraction also depends on the distance between particles, and the number of particles that form a network. Although a high VDW is associated with large-size particles, for ZrO_2 it was found that the strong attraction was due to the high concentration of small-size particles. Consequently, the properties of the fine particles are used to determine the rheological behavior of the colloidal solution (Leong *et al.* 1995)

The pH is another parameter that can highly affect the flow of non-Newtonian fluids more specifically their yield stress. Yield stress can be defined as the minimum shear stress required for the material to display viscous behaviour (Barnes 1999). The yield stress is strongly dependant of the pH of a slurry. It was found that, for different volumetric fraction of a slurry, when the pH is between 5 and 7, the yield stress increases (see Figure 2. 15). This means that there is a tight bond between the particles. On the other hand, when the pH is between 7 and 10, the yield stress decreases, and the particles are dissociated (Leong *et al.* 1995). This is due to the fact that the electrostatic reactions between two particles depend on their natural surface charge that is directly influenced by the pH level. Particles of similar surface charge repel each other. Hence pH is used to regulate the charges. The pH is also a parameter that influences the zeta potential of a suspension (Greenwood *et al.* 2002).

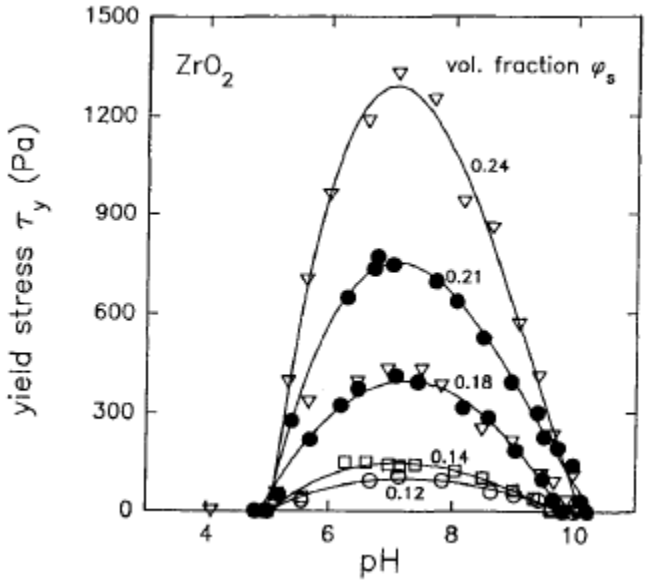

Figure 2. 15- The effect of pH on the yield stress of suspensions (Leong et al. 1995)

Temperature is another parameter that highly affects the rheology of non-Newtonian fluids. It was previously found that the yield stress of a slurry decreases with an increasing temperature. It has also been found that at 50°C a flow transition between shear thinning and shear thickening takes place (He *et al.* 2004).

It has been mentioned that the particle size and its distribution are factors that have impact on the flow of suspensions. Nevertheless, the shape of the particles can have effects as important, especially if the slurry is predominantly solid. He *et al.* 2004, while studying the slurry rheology of industrial minerals, observed that a spherical halloysite provokes lower viscosity while kaolinite and tubular halloysite result in higher viscosity (He *et al.* 2004).

2.3.4 Physical and Chemical Properties

Rust, corrosion by-product, has a lower density than the parent iron and therefore occupies more volume. Experimental studies have proven that all iron oxide phases have different densities. Therefore, density is the property with which the chemical status and the degree of oxidation of CP can be identified.

The rust expansion coefficient (R_v) is the volumetric ratio of rust products to parent iron. R_v is a function of environmental and chemical factors. According to the literature, R_v increases with the supply of oxygen and high humidity (Zhao *et al.* 2012). Table 2. 3 lists the rust expansion coefficient for several iron oxide phases. Within the three most common phases in RC corrosion, hematite, magnetite and lepidocrocite have expansion coefficient between 2.0 and 3.0 (Zhao *et al.* 2012). Therefore, the range of values for R_v recommended for modelling corrosion-induced cracking of the concrete cover is between 2.0 and 3.0 (Suda *et al.* 1993).

Table 2. 3- Corrosion products expansion coefficient (Balafas and Burgoyne 2011)

Name	Chemical Formula	Rust Expansion Coefficient (R_v)
Iron oxide	FeO	1.7
Hematite	$\frac{1}{2}Fe_2O_3$	2.12 (Caré et al. 2008)
Magnetite	$\frac{1}{3}Fe_3O_4$	2.08 (Caré et al. 2008)
Goethite	$\alpha - FeOOH$	2.91 (Caré et al. 2008)
Akageneite	$B - FeOOH$	3.48 (Caré et al. 2008)
Lepidocrocite	$\gamma - FeOOH$	3.03 (Caré et al. 2008)
Ferrous Hydroxide	$Fe(OH)_2$	3.75
Ferric Hydroxide	$Fe(OH)_3$	4.2
Hydrated Ferric Oxide	$Fe(OH)_3, 3H_2O$	6.4

Andrade (2013) observed that the expansive character of CP comes from their ability to retain water. When dried, rust does lose all its stiffness and undergoes shrinkage. This means that any measurement of expansion or density must be done while the corrosion products are still wet. The author states how temperature affects R_v (Andrade 2013). In another study, Molina *et al.* (2013) assumed that the value of R_v changes linearly with time when used in FE modelling.

The chemical properties of corrosion products are as important as the physical properties. They can be determined by using material characterization methods such as Fourier Transform Infrared Spectrometer (FTIR), Moss Bauer spectroscopy, X-ray micro-computer tomography, Raman spectroscopy, X-ray diffraction (XRD) or X-ray fluorescence (XRF).

FTIR measures trends and reaction profiles in real time, providing very specific information on the kinetics, mechanism and the influence of variables on chemical reactions. With this method, it is possible to identify the elemental phases of the sample, including details on reactions in progress. This method is useful to characterize corrosion products as it will help follow their progress during the transformation from iron to iron oxide. It also helps determine the elemental analysis of CP. In a study by Yahya *et al.* (2008), corrosion products were tested with FTIR, and the results demonstrated that the rust transformation formation rate was in the following order:

Lepidocrocite > magnetite > goethite

Hence, goethite and magnetite were considered to be the transition phases of corrosion products, and lepidocrocite the final by-product of reinforcement corrosion (Yahya *et al.* 2008).

In 2007, a new relation was discovered through FTIR (Gotić and Musić 2007). The conclusions stated that iron oxide reacts and absorbs sulphates when it is in a low pH, acidic environment. Therefore, the destruction of the passive layer between the reinforcement bar and the concrete can be detected with the chemical properties of corrosion products (Gotić and Musić 2007). The reliability of FTIR was put in question. Veneranda *et al*. (2018) studied the chemical and elemental properties of iron oxide with XRD and FTIR to evaluate both methods. The study concluded that both methods are as efficient; however, FTIR has the advantage of executing crystalline analysis with a small amount of sample.

Moss Bauer is a spectroscopy method used to study the chemical reaction of a solution. Studies conducted using this method support the results presented in this literature review. The spectroscopy spectra show the presence of magnetite, goethite and lepidocrocite, each characterized by their different hyperfine parameters (Gotić and Musić 2007; Oh *et al.* 1998; Aperador *et al.* 2011).

2.4 Effect of Corrosion Products on Reinforced Concrete

2.4.1 Concrete: A Porous Medium

A porous medium can be defined as a solid that contains space to hold a fluid. Concrete is an excellent example of a porous medium. The pores that exist in this medium can be open pores, closed pores or partially open porous as shown in Figure 2. 16. Only the open pores can contribute to the flow of the fluid within the solid. Another important characteristic of pores that should always be considered is their interconnectivity. Fenestration is a connection that is created between adjacent pores. Moreover, tortuosity is the ratio of the actual path length of the flow to its length of displacement. These variables have crucial effects on the transportation of fluids and should be given special attention while studying the behavior of CP and their movement within the concrete matrix.

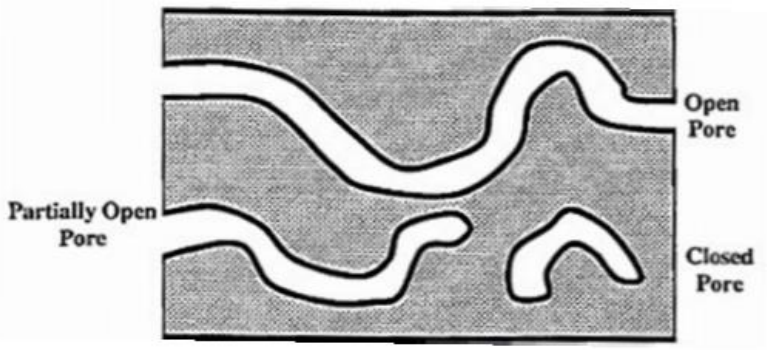

Figure 2. 16- Types of pores in porous media (Foruzanmehr 2019)

Inaccessible pore volumes are volumes where the fluids do not have access to enter. It occurs when the size of the fluid molecule becomes the same order of magnitude as the pore size. This phenomenon will highly affect the flow of the fluids especially if the fluid is highly viscous.

The interaction between visco-plastic fluids and porous media is highly complex, especially because some parameters make it so that the flow is either controlled or behaves in different ways. Adsorption, mechanical entrapment and inaccessible pore volume can be cited as some of these phenomena.

According to Power's law, the porosity of concrete is directly related to the water-to-cement ratio of concrete (Powers et *al.* 1954). The Canadian Standard Association (CSA A23.1-14/A23.1-14) specifies the maximum water-to-cement ratio of a concrete mix depending on the environmental conditions (CSA A23.1-14 2014). Chen and Wu (2013) related the water-to-cement ratio of a concrete mix to the pore diameter and the cumulative intruded pore volume. Figure 2. 17 shows that the cumulative intruded pore volume increases with w/c.

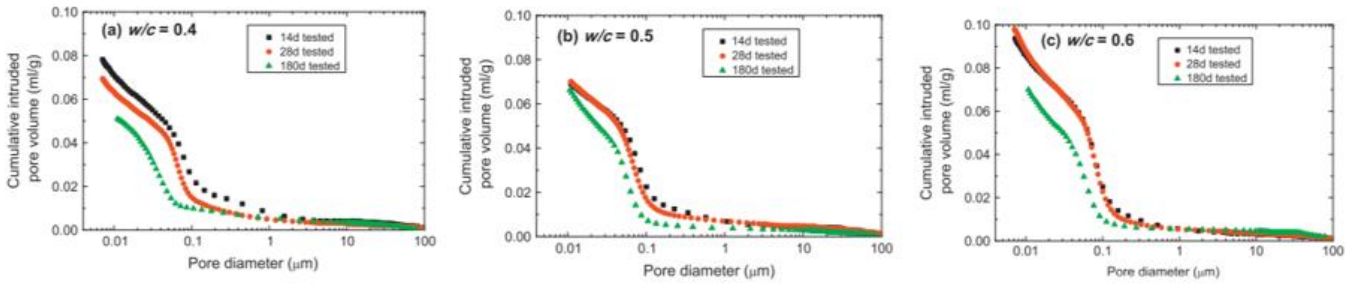

Figure 2. 17- Pore diameter for varying water-to-cement ratio (Chen and Wu 2013)

In order to characterize corrosion products in RC, multiple researchers have considered a single w/c of 0.5 (Vera *et al.* 2009; Pacheco and Polder 2012).

2.4.2 Distribution of Corrosion Products around Rebars

The distribution of CP around rebars is difficult to determine; almost all modelling attempts and studies have been based on the assumption that corrosion products are distributed uniformly. However, it has already been proven that this is not the reality as seen in Figure 2. 2 and Figure 2. 3. Studies have also shown, with SEM, that there are two main layers of rust that are formed around the rebars. First, a thin layer of mill scale or a flaky surface of iron oxide is present in contact with the steel. Around the thin layer, another layer of corrosion product is present. The mill scale does not contribute to the corrosion process, so its thickness is usually subtracted from the overall rust thickness (Zhao *et al.* 2012).

A study by Suda *et al.* (1993) has proven that the corrosion products occur in layers both in bare bars and within concrete. Along the same line, it was observed that the thickness of CP for concrete embedded bars is much less than the thickness for bare bars. The thickness of rust layers in embedded bars was found to be between 180 and 1,300 μm. Furthermore, 30% of the rust is composed of crystalline magnetite, goethite and lepidocrocite, while the rest is occupied by the amorphous portion (Suda *et al.* 1993).

2.4.3 Propagation of Corrosion Products through Concrete Cracks

After the creation of the first concrete cracks during the propagation stage of corrosion, it is very important to study how the rust behaves when it travels through the cracks. The transport of corrosion products plays an important role in the concrete's level of damage. It was proven by researchers that the cracks formed in RC do not follow a certain pattern (Keivan and Hossein 2011). They all have different thickness length and direction. As assumed by Keivan and Hossein (2011), in a porous reinforced concrete sample, CP migrate through the pores and micro cracks of concrete towards the outside of the concrete cover to become visible. The rust is brought to the surface of the concrete cover by a convection and diffusion process that creates movement. In order to model the rust movement through the cracks, multiple assumptions were made, as stated below:

- The rebar corrosion occurs uniformly on its surface along a sizeable length
- The mechanical behavior of steel, rust, and concrete are considered to be linear isotropic.
- The RC concrete cover is idealized as a thick-walled cylinder subject to internal pressure. The cylinder is assumed to be so long that any plane transverse section remains plane under rebar corrosion." (Keivan and Hossein 2011).

The assumption that the corrosion products never create expansive pressure on the concrete cover before all the porous zone around the steel/concrete is filled rejected by Zhao *et al.* (2012). This group of researchers observed that the corrosion products penetrate the cracks even before filling out all the pores (Zhao *et al.* 2012)Therefore, according to this study, the stage in which rust fills the porous zone and where it creates expansion pressure must be analysed in parallel instead of separately.

Other studies have focused on the relation between the transport of corrosion products and the cracks. Sola *et al.* (2019) were able to prove that the distribution and penetration of corrosion products through cracks is dependent on the crack saturation and spacing and width. Moreover, other studies have concluded that the corrosion products found around the rebars and in between cracks do not behave the same. The iron oxide in cracks is said to behave as anodes, whereas the iron oxide around the rebars behave as cathodes. However, this does not have any effect on the corrosion rate or the corrosion related reactions (Pacheco and Polder 2012).

2.5 Gaps in the State-of-the-Art

Bases on the literature review presented, here is a list of important aspects and gaps in the state-of-the-art.

1. There is not a standard laboratory procedure to produce corrosion products. Different methods have been tested in the laboratory and in the field (Suda *et al.* 1993; Konopka 2005; Ouglova *et al.* 2006; Balafas and Burgoyne 2011; Zhao *et al.* 2012; Andrade 2013).
2. The nature of corrosion products in concrete is yet to be determined as multiple researchers have adopted different assumptions (Molina *et al.* 1993; Lundgren and Gylltoft 2009; Ouglova *et al.* 2006; Andrade 2013)
3. Different material characterization methods have been used as an attempt to determine the properties of corrosion products by research (Suda *et al.* 1993; Gotić and Musić 2007; Jaffer and Hansson 2009; Vera *et al.* 2009).

4. The main iron oxide phases that are identified in corrosion products are goethite, magnetite and lepidocrocite (Oh *et al.* 1998; Antunes *et al.* 2003; Gotić and Musić 2007; Jaffer and Hansson 2009)
5. There is a contradiction in the study of the rheological behavior of corrosion products whereas some have assumed that CP behaves as Newtonian material (Ouglova *et al.* 2006), others as non-Newtonian (Molina *et al.* 1993; Andrade and Alonso 2001).
6. The pH, particle size, particle distribution, particle morphology and temperature are factors that highly impact the rheological behavior of non-Newtonian fluids. They all have to be considered while studying CP (Leong *et al*. 1995; Greenwood *et al.* 2002; He *et al.* 2004)
7. More research is needed to understand the rheological behavior of CP and its effect on reinforced concrete. It is important to analyze how CP acts as a fracturing liquid and how corrosion-induced cracks are created in RC.

The purpose of this thesis is to fill the gaps that exist in the literature up to date. The following chapters will be dedicated to providing experimental analysis in regard to this subject. By putting together existing data and producing new experimental one, this thesis will be able to clarify and characterize the nature and behavior of corrosion products in reinforced concrete.

2.6 References

ACI Committee 201. 2008. 201.2R-08 Guide to Durable Concrete. American Concrete Insitute.

ACI Committee 201. 2016. 201.1R Guide for Conducting a Visual Inspection of Concrete in Service. American Concrete Institute.

ASTM international G15 -08, Standard terminology relating to corrosion and corrosion testing, n.d. https://compass.astm.org/download/G15-WITHDRAWN.19604.pdf.

Andrade, C. (2013). "Oxide formation due to rebar corrosion and its relation to cover cracking." *8th International Conference on Fracture Mechanics of Concrete and Concrete Structures*. Post Conference Workshop - 14 March 2013

Antunes, Renato Altobelli, Isolda Costa, Dalva Lúcia, and Araújo De Faria. 2003. “Characterization of Corrosion Products Formed on Steels in the First Months of Atmospheric Exposure 403 Characterization of Corrosion Products Formed on Steels in the First Months of Atmospheric Exposure.” Materials Research. Vol. 6.

Aperador, Willian, Jorge Bautista, and Enrique Vera. 2011. “Mossbauer and XRD Analysis of Corrosion Products of Carbonated Alkali-Activated Slag” 78: 198–203.

Balafas, Ioannis, and Chris J. Burgoyne. 2011. “Modeling the Structural Effects of Rust in Concrete Cover.” Journal of Engineering Mechanics 137 (3): 175–85. https://doi.org/10.1061/(ASCE)EM.1943-7889.0000215.

Barnes, Howard A. 1999. “The Yield Stress - a Review - Everything Flows?” Journal of Non-Newtonian Fluid Mechanics 81 (1–2): 133–78. https://doi.org/https://doi.org/10.1016/S0377-0257(98)00094-9.

Bertolini, Luca. 2008. “Steel Corrosion and Service Life of Reinforced Concrete Structures.” Structure and Infrastructure Engineering 4 (2): 123–37. https://doi.org/10.1080/15732470601155490.

Chen, Xudong, and Shenxin Wu. 2013. “Influence of Water-to-Cement Ratio and Curing Period on Pore Structure of Cement Mortar.” Construction and Building Materials 38 (January): 804–12. https://doi.org/10.1016/j.conbuildmat.2012.09.058.

COWI. 2017. “Status of the Champlain Bridge Ensuring Safety and Mobility through Rigorous and Constant Monitoring.” www.JacquesCartierChamplain.ca.

CSA A23.1-14. 2014. “Concrete Materials and Methods of Construction/ Test Methods and Standard Practices for Concrete.”

Foruzanmehr, Reza. 2019. “Porosimetry • CVG 6310 Characterization Methods for Materials.”

Gotić, Marijan, and Svetozar Musić. 2007. “Mössbauer, FT-IR and FE SEM Investigation of Iron Oxides Precipitated from FeSO4 Solutions.” Journal of Molecular Structure 834–836 (SPEC. ISS.): 445–53. https://doi.org/10.1016/j.molstruc.2006.10.059.

Greenwood, R, N Rowson, S Kingman, and G Brown. 2002. “A New Method for Determining the Optimum Dispersant Concentration in Aqueous Grinding.” Powder Technology 123: 199–207. www.elsevier.comrlocaterpowtec.

He, Mingzhao, Yanmin Wang, and Eric Forssberg. 2004. “Slurry Rheology in Wet Ultrafine Grinding of Industrial Minerals: A Review.” Powder Technology 147 (1–3): 94–112. https://doi.org/10.1016/j.powtec.2004.09.032.

Jaffer, Shahzma J., and Carolyn M. Hansson. 2009. “Chloride-Induced Corrosion Products of Steel in Cracked-Concrete Subjected to Different Loading Conditions.” Cement and Concrete Research 39 (2): 116–25. https://doi.org/10.1016/j.cemconres.2008.11.001.

Keivan, Kiani, and M.Shodja Hossein. 2011. “Prediction of the Penetrated Rust into the Microcracks of Concrete Cause by Reinforcement.” Applied Mathematical Modelling volume 35: 2529–43.

Konopka, P. 2005. “Structural Properties of Rust. 4th-Year Undergraduate Project.” Cambridge, UK.

Kosmatka, Steven H., Beatrix Kerkhoff, William C. Panares, Norman F. MacLeod, and Rivhard J. McGrath. 2002. Design and Control of Concrete Mixture. 7th edition. Ottawa, Ontario, Canada: Cement Association of Canada.

Leong, Yee-Kwong, Peter J Scales, Thomas W Healy, and David V Boger. 1995. "Effect of Particle Size on Colloidal Zirconia Rheology at the Lsoelectric Point." *Am. Ceram. SOC*. Vol. 78.

Liu, Youping, and Richard E Weyers. 1998. "Modeling the Time-to-Corrosion Cracking in Chloride Contaminated Reinforced Concrete Structures." ACI Materials Journal 95 (6): 675–81.

Lundgren, Karin. 2002. "A Model for the Bond Between Corroded Reinforcement and Concrete." Chalmers University of Technology.

Lundgren, Karin, and Kent Gylltoft. 2009. "A Model for the Bond between Concrete and Reinforcement." Magazine of Concrete Research 52 (1): 53–63. https://doi.org/10.1680/macr.2000.52.1.53.

Molina, F J, C Alonso, and C Andrade. 1993. "Cover Cracking as a Function of Rebar Corrosion: Part 2 Numerical Model." Materials and Structures 26: 532–48.

Oh, Sei J., D.C. Cook, and H.E. Townsend. 1998. "Characterization Of Iron Oxides Commonly Formed As Corrosion Products On Steel." https://doi.org/10.1023/A:1011076308501.

Ouglova, A., Y. Berthaud, M. François, and F. Foct. 2006. "Mechanical Properties of an Iron Oxide Formed by Corrosion in Reinforced Concrete Structures." Corrosion Science 48 (12): 3988–4000. https://doi.org/10.1016/j.corsci.2006.03.007.

Pacheco, José, and Rob Polder. 2012. "Corrosion Initiation and Propagation in Cracked Concrete - a Literature Review." RILEM Bookseries. https://doi.org/10.1007/978-94-007-2703-8_9.

Powers, T. C., J. C. Copeland, J. C. Hayes, and H. M. Mann. 1954. "Permiability of Portland Cement Paste." American Concrete Insitute 51 (11): 285–98.

Powers, T. C., J. C. Copeland, and H. M. Mann. 1970. "Capillary Continuity or Discontinuity in Cement Pastes." Portland Cement Association 5 (0): 110.

Qiao, Di, Hikaru Nakamura, Yoshihito Yamamoto, and Taito Miura. 2016. "Crack Patterns of Concrete with a Single Rebar Subjected to Non-Uniform and Localized Corrosion." Construction and Building Materials 116 (July): 366–77. https://doi.org/10.1016/j.conbuildmat.2016.04.149.

Robotti, Nadia. 2013. "The Discovery of X-Ray Diffraction." In Rendiconti Lincei. Vol. 24. https://doi.org/10.1007/s12210-012-0205-1.

Sola, E., J. Ožbolt, G. Balabanić, and Z. M. Mir. 2019. "Experimental and Numerical Study of

Accelerated Corrosion of Steel Reinforcement in Concrete: Transport of Corrosion Products." *Cement and Concrete Research* 120 (June): 119–31.

Suda, Kumiko, Sudhir Misra, and Kenichi Motohashi. 1993. "Corrosion Products of Reinforcing Bars Embedded in Concrete." Corrosion Science 35: 1543–49.

Tilly, Graham. 2007. "The Durability of Repaired Concrete Structures.," 1–8. https://doi.org/10.2749/222137807796120030.

Trejo, David, Naga Pavan Vaddey, and Mahmoud Shakouri. 2019. "Factors Influencing Chloride Test Results of Cementitious Systems." ACI Materials Journal 116 (1): 135–45. https://doi.org/10.14359/51712240.

Tuutti, Kyosti. 1982. Corrosion of Steel in Concrete. Stockholm: Swedish Cement and Concrete Research Institute.

Vera, R., M. Villarroel, A. M. Carvajal, E. Vera, and C. Ortiz. 2009. "Corrosion Products of Reinforcement in Concrete in Marine and Industrial Environments." Materials Chemistry and Physics 114 (1): 467–74. https://doi.org/10.1016/j.matchemphys.2008.09.063.

Yahya, Solhan, Affaizza Mohamad Shah, Afidah Abdul Rahim, Nursila Hanim, Abd Aziz, and Rozieyanie Roslan. 2008. "Phase Transformation of Rust in the Presence of Various Tannins." Journal of Physical Science. Vol. 19.

Zhang, Weiping, Junyu Chen, and Xujiang Luo. 2019. "Effects of Impressed Current Density on Corrosion Induced Cracking of Concrete Cover." Construction and Building Materials 204 (April): 213–23. https://doi.org/10.1016/j.conbuildmat.2019.01.230.

Zhao, Yuxi, Hong Dai, and Weiliang Jin. 2012. "A Study of the Elastic Moduli of Corrosion Products Using Nano-Indentation Techniques." Corrosion Science 65 (December): 163–68. https://doi.org/10.1016/j.corsci.2012.08.016.

Zhao, Yuxi, Hong Dai, Haiyang Ren, and Weiliang Jin. 2012. "Experimental Study of the Modulus of Steel Corrosion in a Concrete Port." Corrosion Science 56 (March): 17–25. https://doi.org/10.1016/j.corsci.2011.11.004.

Zhao, Yuxi, Yingyao Wu, and Weiliang Jin. 2013. "Distribution of Millscale on Corroded Steel Bars and Penetration of Steel Corrosion Products in Concrete." Corrosion Science 66: 160–68. https://doi.org/10.1016/j.corsci.2012.09.014.

Zhao, Yuxi, Jiang Yu, Yingyao Wu, and Weiliang Jin. 2012. "Critical Thickness of Rust Layer at Inner and out Surface Cracking of Concrete Cover in Reinforced Concrete Structures." Corrosion Science 59 (June): 316–23. https://doi.org/10.1016/j.corsci.2012.03.018.

Chapter 3

3. Investigation of the crystalline, rheological, and physical properties of iron oxide phases in corrosion products

3.1 Abstract

This paper aims to study the evolution of the rheological behaviour of corrosion products (CP) in a high alkaline environment to understand corrosion-induced fracture in reinforced concrete due to reinforcement corrosion. A mixture of iron powder, sodium chloride, calcium hydroxide, and water is used to produce corrosion products. The development of CP is studied at 2, 4, 6- and 8-week intervals. Imaging techniques along with rheological characterization methods were conducted to understand the viscoelastic flow behavior of CP. The results show that CP exhibits different rheologic properties through the corrosion process. Three iron oxide phases (magnetite, goethite, and lepidocrocite) have been detected throughout the initiation and propagation stages of corrosion. The corrosion products obtained for each study period are found to behave as colloidal materials, demonstrating all the characteristics of shear-thinning materials. In addition, as a result of the chemical and particle disintegration, the viscosity of CP decreases with the applied shear rate. The experimental data also showed that the density of corrosion products and their particle size decreased with time.

3.2 Introduction

Reinforcement corrosion is the most common deterioration mechanism in reinforced concrete (RC), compromising the serviceability limit state, and in some cases, the ultimate limit state of RC structures (Tilly 2007). As reinforcement corrosion initiates and propagates, corrosion products

(CP) are formed through electrochemical reactions. Researchers have assumed the CP to behave as solid material (Ouglova *et al.* 2006; Lundgren 2002). However, this paper, along with others, have shown that CP behaves as an expansive colloidal material (Andrade 2013). The corrosion by-product has distinct behaviors; when CP penetrates through a porous media, it can act as a hydraulic fracturing fluid. It is also known to have a lower density (3,970 kg/m^3 – 4,345 kg/m^3) in comparison with the original reinforcement steel (7,850 kg/m^3) (Ouglova et al. 2006). The gradual decrease in density leads to an increase in volume, exerting pressure in the surrounding concrete and eventually provoking the concrete cover to crack when its tensile capacity has been reached. The cracks that appear are driven by a phenomenon similar to that of hydraulic fracturing. The build-up of CP acts as a hydraulic pump to surrounding porous media. Therefore, the concrete cover is pressurized to crack. Simultaneously, rust permeates the cracks instigating additional tensile stresses and causing the propagation of cracks. In other words, fractures and cracks are formed in a porous media subject to constant stress. Under these conditions, pressure is transferred and a weaker concrete to steel interaction is introduced.

In fact, the rheological properties of fracturing fluids such as the CP have a significant impact on hydraulic-induced fracturing. The viscosity and the range of shear rate associated with the highest variation of viscosity have a vital effect on the penetration and the evolution of the fluids through the fracture (Wrobel *et al.* 2021). Researchers have shown that for high-viscosity fluids, a high level of pressure is obtained through the cracks. The type of fracture is also highly impacted by the rheology of the fluid. For example, for viscous fluids, the cracks are most likely to be short, branched, and tortuous (Bohloli *et al.* 2006). In addition, the morphology, particle size distribution, and rheology of fracturing fluids determine the stability and the proppant suspension capacity of the fluid. The stability of a fracturing fluid is an important factor to study because it is indicative of the contact angles between the fluid and the media surrounding it. The proppant suspension capacity is used to evaluate the solid transportation capacity of the liquid through the fractures (Verma *et al.* 2018).

The rheological behavior of the CP can determine the pattern of the cracks formed in RC. The experimental investigations available in the literature have shown different rheological and physical behavior of CP. Many possibilities have been taken into consideration, where CP can be modeled as a fluid (Molina *et al.* 1993; Andrade 2013), a suspension (Andrade 2013) or a granular

material (Lundgren 2002; Ouglova *et al.* 2006). CP's rheological behavior is a factor of the type of iron oxide formed during the corrosion process and its water content. There are nine different oxides that can be formed following the oxidization of iron (Oh *et al.* 1998). However, CP in RC is mainly formed of 3 iron oxide phases: magnetite , goethite and lepidocrocite (Gotić and Musić 2007). These iron oxide phases can be identified with their morphology, chemical, and physical properties. The rheological properties of CP at each corrosion stage is a function of pH, particle size and particle concentration and temperature (Leong *et al.* 1995; Greenwood *et al.* 2002; He *et al.* 2004). The rheological behavior of CP determines the pattern of the cracks formed in the concrete cover. For this reason, it is crucial to characterize and understand the nature of CP and how it flows in a high-alkaline porous environment.

The final by-product of steel corrosion, the CP, involves different compounds. Each compound exhibits unique chemical and physical properties most of which can be distinguished by their colors. Nevertheless, when they are not perceptible with their color, imaging techniques can differentiate them (Antunes *et al.* 2003). In order to better understand the rheological behavior of the CP in RC, it is crucial to characterize the physical properties of the CP, such as its crystalline structure, density and morphology. The literature shows that the formation of iron oxide phases depends on the nature of the corrosive environment (Antunes *et al.* 2003). Furthermore, the physical and chemical properties of these phases affect their rheological behavior. Gotić *et al.* observed that different iron oxide phases were formed in different layers on the surface of the reinforcing steel in RC before they start to diffuse through the cracks and concrete matrix (Gotić and Musić 2007). However, there is a gap in the literature concerning the relationship between the physical and chemical status of the CP and its rheological properties.

3.3 Scope of work

There is currently a number of inconsistencies in the literature regarding the rheological properties of CP. The literature has shown various CP definitions: suspension, liquid, or solid (Ouglova *et al.* 2006; Molina et *al.* 1993; Andrade and Alonso 2001). However, there are still several gaps to be filled in the research. Therefore, the purpose of this paper is to characterize and appraise the rheological behavior of CP to better understand the effect of hydraulic-induced fracture in RC. The CP was produced in the laboratory through accelerated corrosion and was studied for a period of 8 weeks. The tests used in this research provided enough information to understand how the CP

behaves in a porous medium. A correlation between the crystalline structure, morphology, density, and rheological properties of CP through its time evolution is determined. Information on the rheological behavior of CP provides quantitative data to be used as input in the modelling of corrosion-infused concrete cover cracking.

3.4 Materials and Methods

3.4.1 Experimental Procedure

To trigger the corrosion electrochemical reactions and reproduce CP in the laboratory, as similar to the naturally occurring corrosion reactions, both stages of corrosion must take place (i.e., initiation and propagation). Iron powder with a purity higher than 99% and with particles of 300 mesh (45-75 microns), was used as the precursor for the reinforcing steel in the CP. Calcium hydroxide was used to provide a high-alkaline environment, similar to the hydrated cement in concrete. Finally, sodium chloride was added to trigger the chloride-induced de-passivation and onset of corrosion. Taking into consideration all the factors that can affect the corrosion process, this study follows the steps below:

1. Preparing a solution of distilled water, 0.5M sodium chloride (to depassivate the steel), and saturated calcium hydroxide (to imitate the alkaline environment of concrete).
2. Introducing 60g of pure iron (Fe) powder to the solution.
3. Introducing air bubbles using two air stone bubblers to promote the oxidation of iron.
4. Stirring the solution every 2 to 3 days.
5. Repeating the experiment at intervals of 2, 4, 6, and 8 weeks.

After 2, 4, 6, and 8 weeks, the samples were collected for tests. The samples were obtained in the form of fine powders by using a vacuum filter (Figure 3.1). The powders were thoroughly washed twice with distilled water to ensure that no impurity remained. At this point, the CP samples were ready to be characterized.

Figure 3. 1- Dried CP produced in the laboratory

3.4.2 Material Characterization Methods

The CP samples were characterized using the following characterization methods listed in Table 3.1. Two samples of each week were used for every measurement.

Table 3. 1- Material characterization methods to evaluate each sample of CP

Methods	Iron Powder	Week 2	Week 4	Week 6	Week 8	Iron oxide powder
XRD	X	X	X	X	X	X
SEM	X	X	X	X	X	X
EDS		X	X	X	X	
Viscometry		X	X	X	X	
Particle size analyzer	X	X	X	X	X	
Gas Pycnometer	X	X	X	X	X	

X-Ray Diffraction

XRD was used to determine the crystalline structure of the CP through the accelerated corrosion process (Zhang *et al.* 2019). XRD spectra were recorded using the Ultima IV diffractometer with a general-purpose theta-theta system with a copper source and one diffracted beam monochromator and a 2-tetha scanner rotated between 0 and 90 degrees with a 40 kV (44 mA) Cu

X-ray continuous source of light. The diffraction spectra were obtained directly on the specimen surface, and the distance between the beam source and the sample was kept equal to the distance from the sample to the detector. Three to five grams of each batch of CP samples were finely ground in order to obtain a uniform particle size. The position and intensity of the reference peaks need to match the data. The peaks were identified and confirmed using the Rigaku XRD software. This software automatically matches all the peaks on the graph with a reference graph of a specific element. If the software detects a peak that can match multiple elements, it presents all the options, and the user chooses the elemental phase that can best represent the sample. To limit the source of errors, references from the Inorganic Crystal Structure Database (ICSD) were used to match the peaks and confirm results manually.

Scanning Electron Microscopy (SEM)

SEM is used to characterize the morphology of the CP and its penetration behavior in the concrete cover's pores and cracks.

A JSM -7500F FESEM SEM with a secondary electron detector (SE) and an acceleration voltage of 3 kV was carried out to study the morphology of the CP samples. This analysis was done in 3 steps: first, 1 to 2 mg of CP was used from each sample batch (week 2 to week 8). Pure iron and iron oxide powders were also used as control samples. Each powder was then mounted on a sample holder with an adherent. Since corrosion powder is a nonconductive material, a 15-μm bench-top ion-based gold coating had to be used on the surface of each sample holder. To degasify the samples, they were put in a 10-8 Torr Vacuum before the SEM.

Energy Dispersive Spectroscopy (EDX)

The same machine and sample preparation methods as SEM were applied for EDX.

Viscometry

The viscosity of CP was measured using an HA viscometer by Can-Am Instruments Ltd. (spindle #6 as shown in Figure 3.2 was used). To ensure that the measurements were not affected by the sample preparation, the particle size, the pH and the temperature were checked. A mortar and pestle were used to assure the uniformity of the particle size for all batches. The pH was regulated between 12.5 and 13 by adding calcium hydroxide, and the samples were kept at room temperature. The rheological behaviour is dependent on the amount of water in CP. To obtain a paste-like

material (or slurry) from the CP powder, distilled water was added; 60 mL of distilled water was mixed with 100g of CP, which was found to give the right consistency of the paste, with no excess water or clumps of solid as seen in Figure 3.3. For the CP samples from week 2, 4, 6 and 8, the shear stress measurements were taken from 5 to 60 rpm with an interval of 10 rpm. However, for the Week 2, the measurements had to be stopped at 50 rpm as the shear stress values were beyond the capacity of the viscometer. The cubic spline interpolation method was applied to determine the unknown values between each interval of measurement.

Figure 3. 2- HA spindle #6 [17]

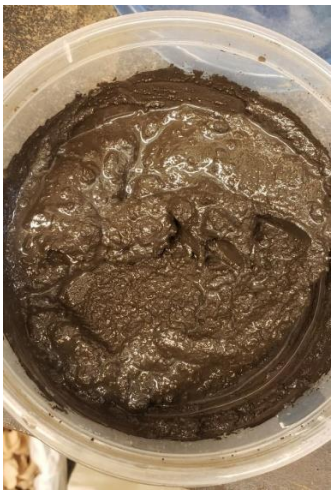

Figure 3. 3- CP paste for viscosity measurement

Mini Slump Test

A mini slump test was conducted to calculate the yield stress of each CP sample. The mini-slump test setup used in this study is a downscaled Abrams cone geometry with 19-mm top diameter, 38-mm bottom diameter and 57-mm height. Each test was performed using a poly (tetrafluoroethene) mini-slump cone on a flat sheet of poly (methyl methacrylate) marked with grid squares (Tan et *al.* 2017). The height and diameter of the CP were measured before and after the test, 5 times for

each sample. The Roussel Spreading Flow describes the yield stress τ (in KPa) as a function of the density of the paste ρ (kg/m^3), the volume of the mini-slump cone Ω (in m^3), and the mini-slump spread diameter R (in m). The yield stress was calculated using the following formula:

$$\tau = \frac{225\rho g \Omega^2}{128\pi^2 R^5} \qquad \textit{Eq 3.1}$$

Particle Size Analysis

After 8 weeks of accelerated corrosion, the samples were washed, dried and re hydrated by adding distilled water. Calcium hydroxide was added to regulate the pH between 12.5 and 13. To measure the particle size of the powders, a Malvern Instrument-Mastersizer 2000 laser particle size analyser was used. Each specimen had to be analysed 2 times for an average result.

Gas Pycnometer Analysis

In order to measure and study the change in the density of the CP over the course of the corrosion evolution, a gas displacement psychometry system (AccPyc ll 1345 Series) developed by Micromeritics was used. Helium was used as the analysis gas.

3.5 Results and Discussion

3.5.1 Crystalline Properties

The XRD experimental data were compared to the crystallographic reference cards to identify the type of iron oxide and its corresponding amounts in the CP. To show how the creation of iron oxides evolve in the CP, the pure iron powder was characterized and used as the control sample. The peaks at 44.8° and 82.4° in Figure 3.4 show the presence of pure alpha iron (Fe). Three major iron oxides of magnetite, goethite and lepidocrocite were identified in the X-ray diffractograms. The planes (220), (422), (511), (440) and (620) were identified for magnetite. Similarly, (120) and (111) are the representative planes for goethite. Goethite is the hydrated version of hematite and is composed of more than 10% water. Lepidocrocite was identified with the planes (200) and (120) on the XRD chart. All three of these oxides have different chemical and crystalline properties (Gotić and Musić 2007).

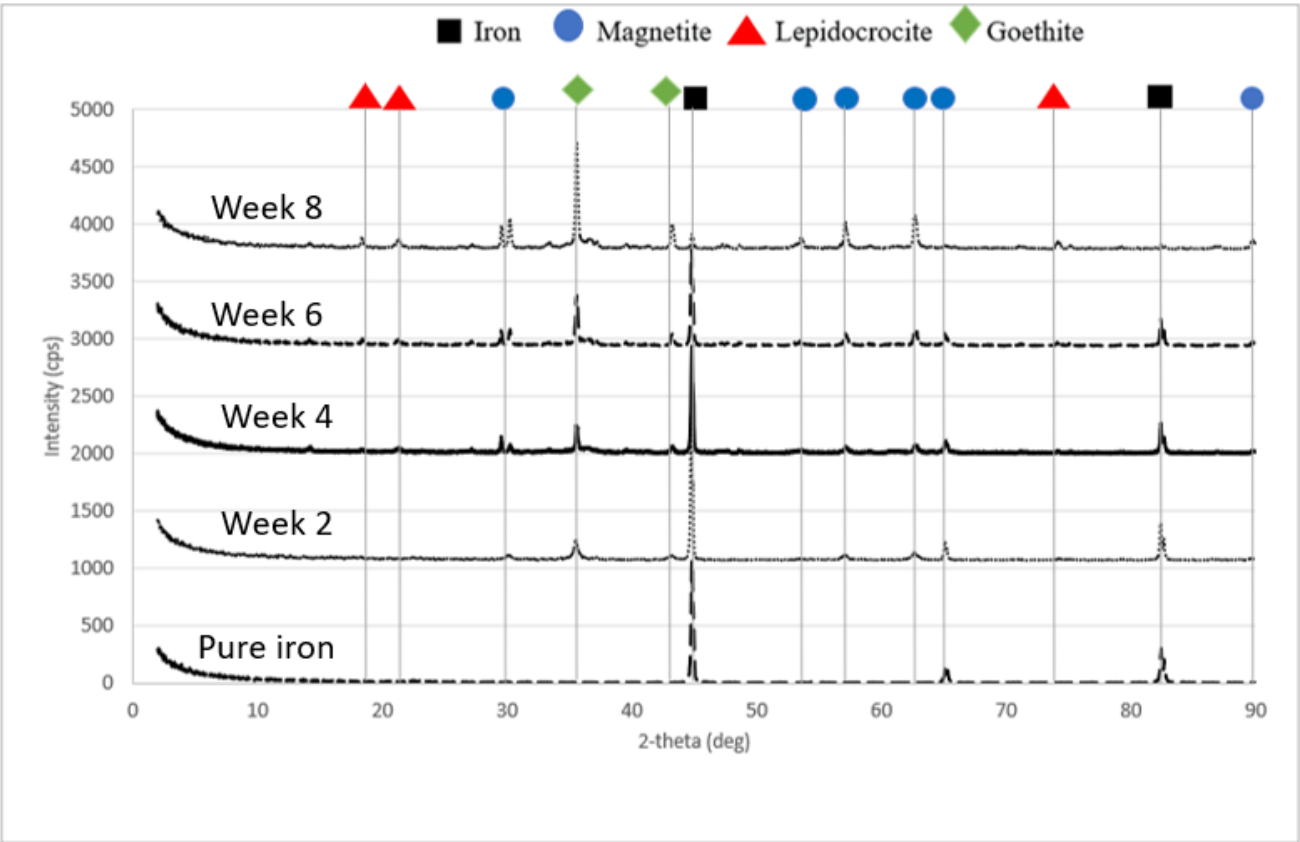

Figure 3. 4- XRD graph for CP

The diffraction peak positions are used to calculate the element's unit cell dimensions. These dimensions are directly related to the interatomic distance as defined by Bragg's Law (Robotti 2013). The width and shape of each peak represent this information on the XRD data graphs. Using these parameters, the amount of each element in a sample was determined. This is what is called a quantitative XRD analysis.

Using the manual analysis, it was also possible to determine the variation of the peak's intensity for all detected phases with time. The results illustrate that from Week 2 to Week 4, the variation is almost negligible. This means that lepidocrocite takes more than 4 weeks to form under accelerated corrosion. The corrosion process is seen to be more active after the 4th week, where the transformation of iron to iron oxide becomes more obvious through the XRD peaks. The majority of oxide transformations took place between the week 6 and week 8 samples, where all peaks show a drastic increase in their intensity. The pure iron oxide sample represented by week

0 has an identical intensity for the peak at 30.2° and a very close intensity for the peak at 62.7° as the corrosion product from the week 8 sample. This shows that the CP produced by the accelerated corrosion process has a similar elemental composition as a pure iron oxide, indicating that the chemical reactions have successfully produced an iron oxide solution. The manual peak identification charts are presented in Appendix A. It is also observed that most of the iron is transformed into iron oxide after 8 weeks of accelerated corrosion as the intensity of iron peaks is fairly negligible for the week 8 sample, as illustrated in Figure 3.5.

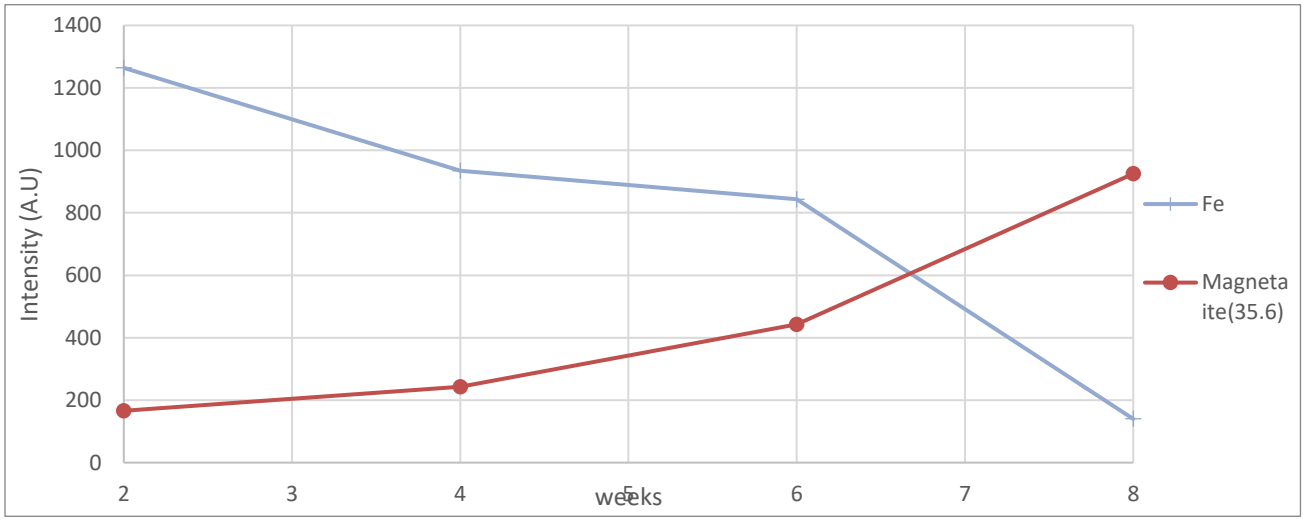

Figure 3. 5- Intensity of iron and magnetite peaks in CP with time

Figure 3.6 shows the evolution of iron oxide phases in the CP with respect to time. For the CP collected in week 2, it is obvious that 50 % of the sample consisted of pure iron and the other 50 percent was magnetite. This indicated that the corrosion process started sometime within the first two weeks of the accelerated corrosion, and more than half of the iron content has been transformed into iron oxide. In Week 4 and 6, magnetite, goethite and lepidocrocite were the three phases that made up the composition of these samples. The appearance of new phases was associated with a significant decrease in the amount of iron. Finally, in Week 8, 90% of the original iron was converted into iron oxide. Yet, iron made up 2.8 % of the sample content. This can be explained by the fact that it may take more than 8 weeks for the accelerated corrosion to exhaust the total content of iron. Generally, ≥90% of CP involves iron oxide phases. The quantitative analyses confirmed that the production of CP commenced at the beginning of Week 2 and reached a maximum plateau somewhere between Week 6 and Week 8.

Calcite ($CaCO_3$) was identified in the CP at the beginning of Week 4. Calcite is a rock-forming mineral and the principal constituent of limestone and marble. The formation of calcite is due to the presence of CO_2, released from the stone air pumps, reacting with the calcium hydroxide in the solution according to the reaction in Eq. 3.1:

$$Ca(OH)_2 + CO_2 \rightarrow CaCO_3 + H_2O \qquad Eq\ 3.2$$

The analysis indicates that magnetite has been the dominant existing iron oxide throughout the whole corrosion process up to the 8th week. The results presented in Figure 3.6 indicate that magnetite (Fe_3O_4) is the iron oxide in greatest quantity at the end of the week 8 of accelerated corrosion, followed by goethite ($Fe_3O(OH)$) and then lepidocrocite ($FeO(OH)$).

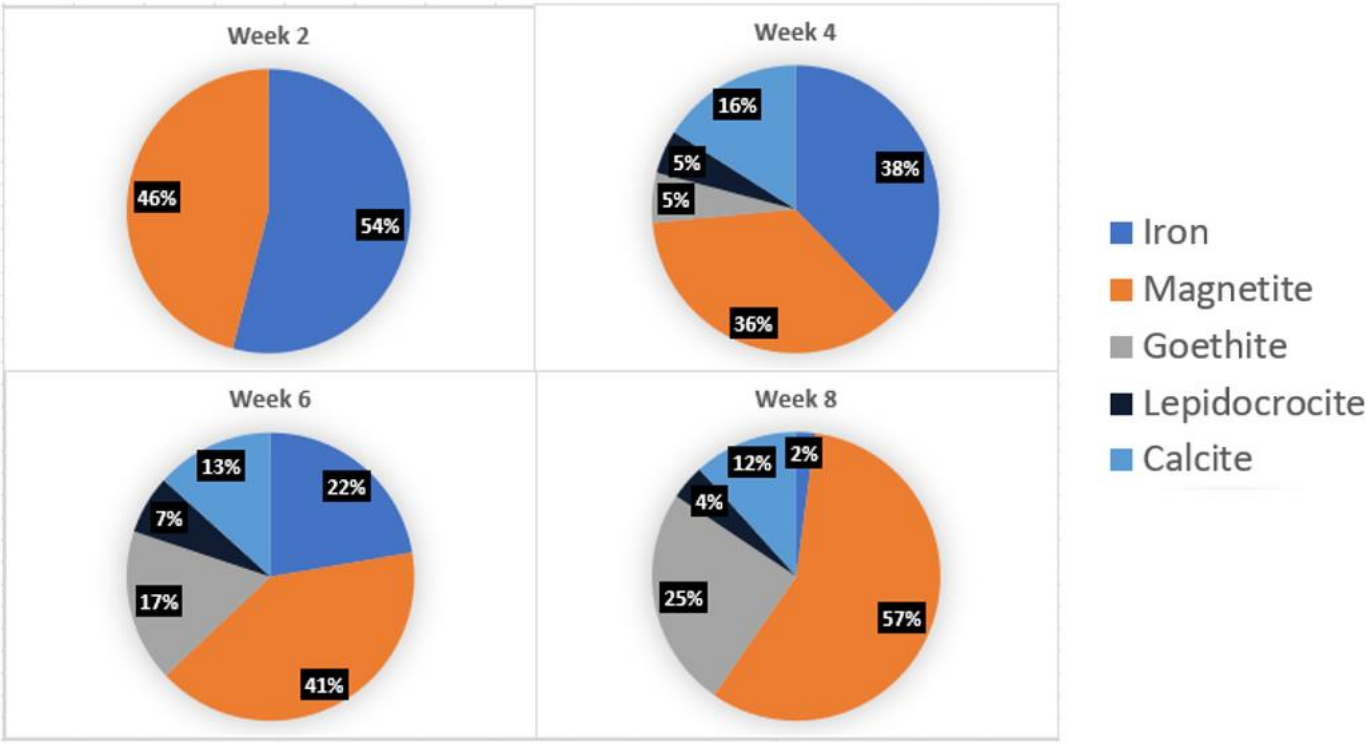

Figure 3. 6- XRD quantitative analysis of CP with time

3.5.2 Elemental Properties

Micrographs of the CP specimens taken by SEM for the week 2-4 samples and the week 6-8 samples are respectively presented in Figure 3. 7 and Figure 3.8. All the particles are of different

size, orientation and shapes. The micrograph for the week 2 sample shows a typical morphology of lepidocrocite. The cauliflower look-alike morphology as well as the sandy crystals in Figure 3.7(a) is representative of lepidocrocite (Ouglova *et al.* 2006). The same structures are visible in the SEM images at Week 4 and Week 8.

The particles in the week 4 sample, Figure 3.7(b) are more in the form of cotton balls of various sizes. Rods of different sizes aggregated into bundles can be seen. Music et *al.* have shown that these are typical representation of goethite and magnetite (Gotić and Musić 2007).

The aggregation process in the week 6 sample, Figure 3.8(a) shows the formation of magnetite particles in various dimensions and shapes (Gotić and Musić 2007). Pyramid looking particles of about 300 nm in size are also visible. In the same micrograph longer goethite rods can also be seen.

The micrograph for the week 8 sample, Figure 3.8(b), displays bundle of rods and plate-like particles along with the morphology of cotton balls. These forms show the presence of goethite (Gotić and Musić 2007). The thickness of goethite plate-like rods is about 2μm on average, whereas the length of goethite short rods is around 1μm. The week 8 sample exhibits a variety of sizes and shapes of goethite particles.

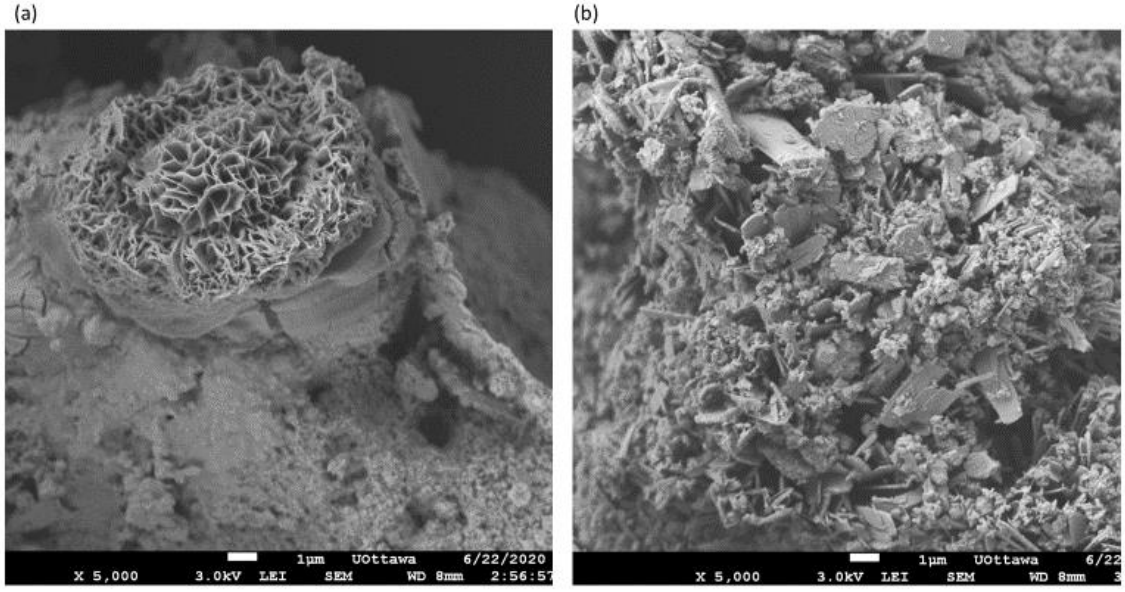

Figure 3. 7- Micrographs of CP at (a) week 2 (b) week 4

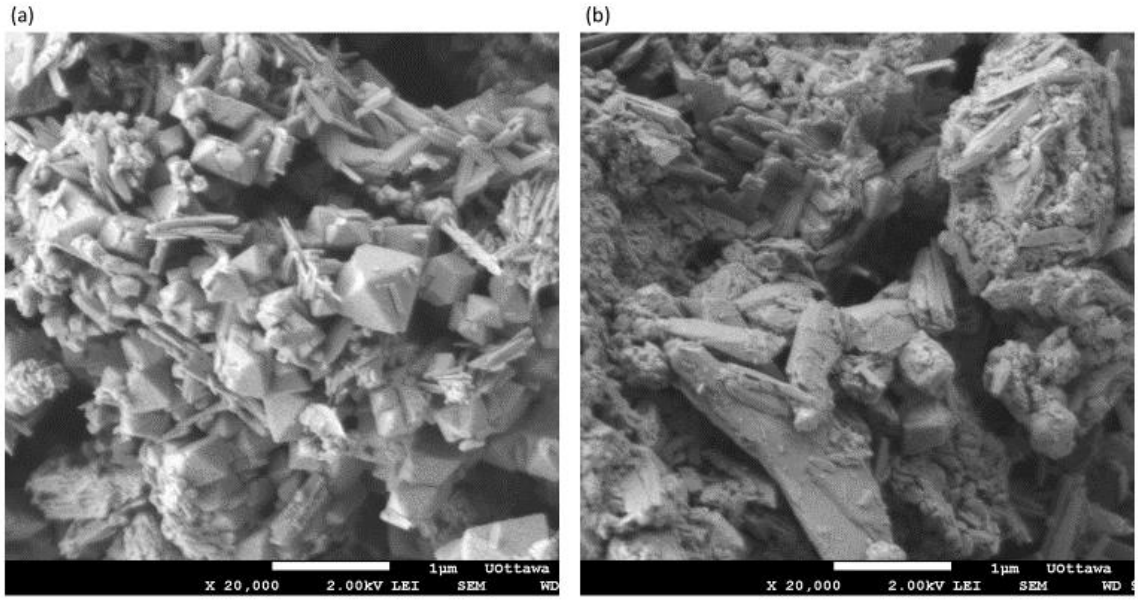

Figure 3. 8- Micrographs of CP at (a) week 6 (b) week 8

These micrographs confirm the results obtained by the XRD analysis. The presence of goethite, magnetite and lepidocrocite are also well observed. The SEM analysis shows that all three oxides are present at every stage of the corrosion process, even for the week 2 sample. This signifies that the electrochemical reactions are active from the start of the experiment. It is also possible to see from the micrographs that the particle size and distribution of CP evolve over the course of the accelerated corrosion process.

Parallel to the SEM analysis, EDX was also conducted to associate each particle seen in the micrographs with its constituent elements. The graphs in Figure 3.9 show the presence of iron (Fe) and oxygen in all 4 samples of CP. There are also Gold (Au) and carbon (C) peaks caused by the coating of the samples. The intensity of the iron peaks is similar for all samples, except for the week 8 sample where it is relatively low because most of the original iron has been transformed by then. The EDX data confirms that there are no additional elements that are present in the CP. These SEM micrographs illustrate that the observed particles are made of a single or various forms of iron oxides.

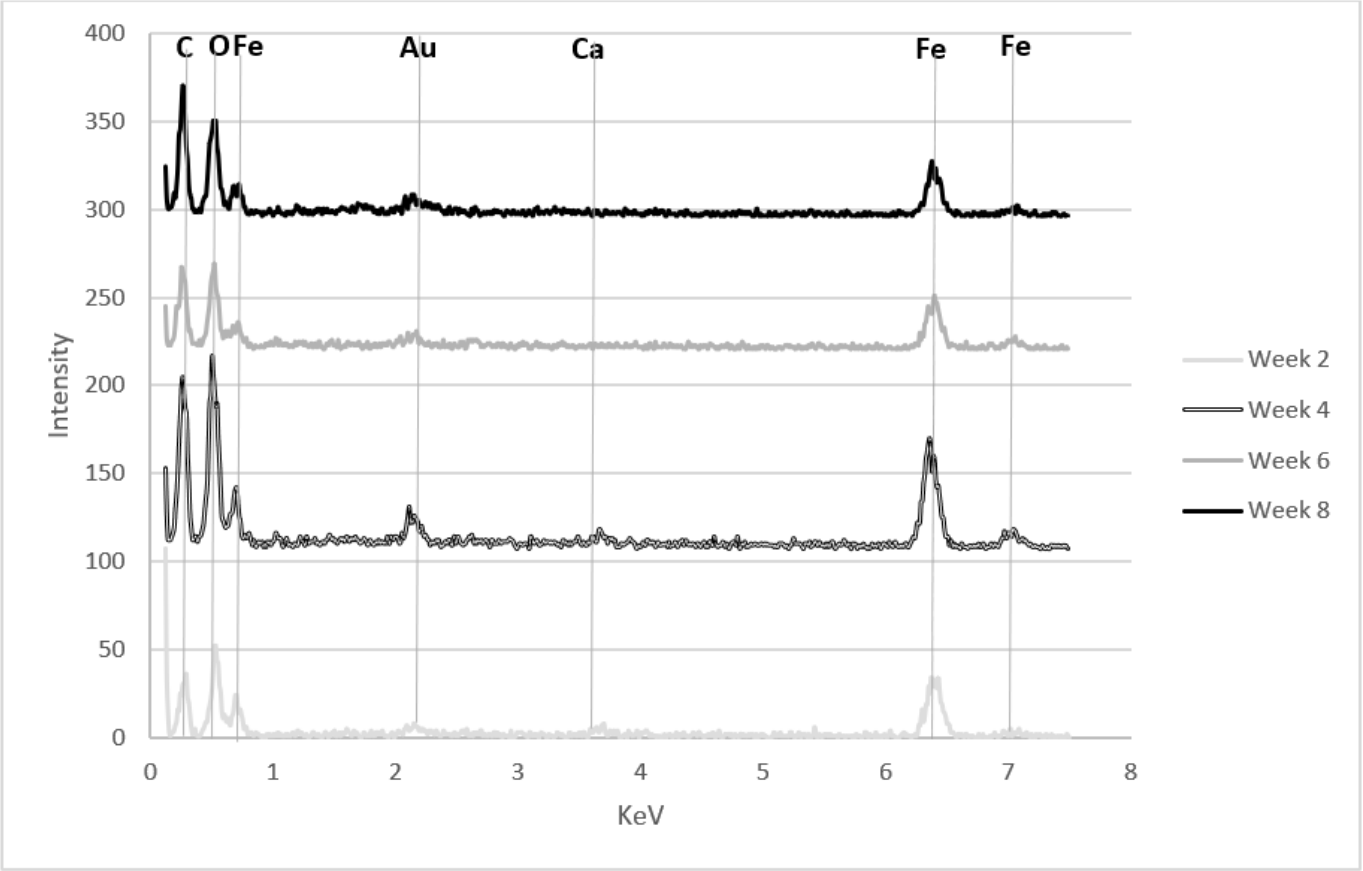

Figure 3. 9- EDS analysis for CP samples

3.5.3 Rheological behavior

SEM micrographs have shown that particles present in the CP exist in different forms and sizes. The effect of particle concentration and particle size on the flow of these types of materials have been studied; Leong et *al.* investigated the effect of particle size on colloidal zirconia rheology (Leong *et al.* 1995). Their study was based on the Van der Waals attraction (VDW) theory, which states that the attraction between two particles is stronger for larger particles. This attraction also depends on the distance between particles and the number of particles that form a network. The average volume per particle size of the CP is shown in Figure 3.10. It can be seen that the particles get smaller in size as time goes by (Figure 3.11). In addition, the greatest difference of particle size occurs between the pure iron samples and the week 2 sample (for particles between 10 and 50μm).

The change in particle size during the corrosion process is indicative that the electrochemical reactions caused the degradation of particles from the pure iron.

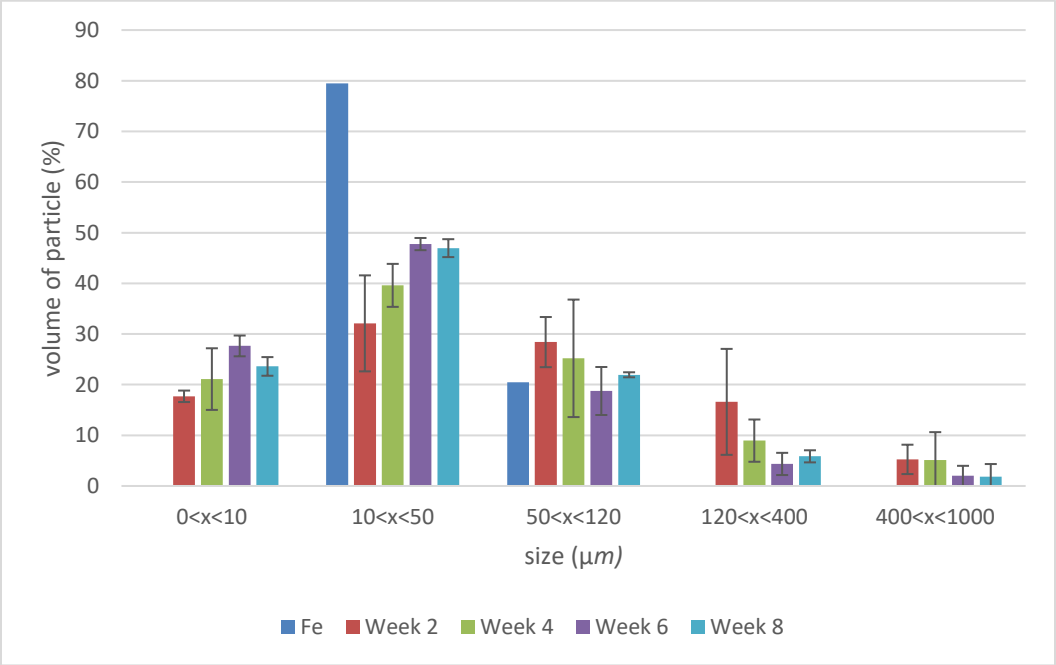

Figure 3. 10- Volume of particles (%) vs particle size (in μm)

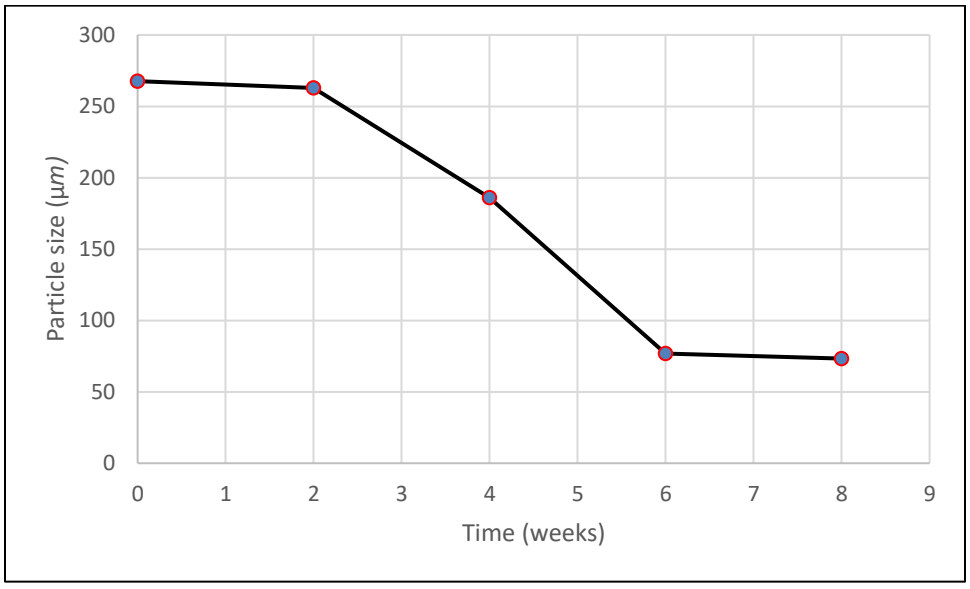

Figure 3. 11- Average particle size of CP with time

The pH is another parameter that greatly affects the rheological behavior of CP. The yield stress is also strongly dependant on the pH of CP. This is due to the fact that the electrostatic reactions

between two particles depend on their natural surface charge that is directly influenced by the pH level (Leong *et al.* 1995).

The magnitude of the viscosity of viscoelastic fluids is dependent on the size and volume of the suspension, spatial distribution of particles, entanglement density, and the molecular arrangement, but most importantly the shearing history of the material. Non-Newtonian fluids can be shear thinning or shear thickening. For shear-thinning fluids, the apparent viscosity decreases with increasing shear rate. In other words, the harder the fluid is sheared, the less viscous it becomes. On the contrary, for shear-thickening fluids, the apparent viscosity increases with increasing shear rate.

The shear stress versus the shear rate plots of the week 2, 4, 6 and 8 samples are presented in Figure 3.12. All four graphs in Figure 3.12 display hysteresis loops. The ascending curves in blue show that as the shear rate increases, the samples behave as non-Newtonian materials. In other words, the CP is a shear-thinning fluid with thixotropic characteristics. The descending curves in red show that shear stress decreases with the shear rate. The plots show a loop test where the shear stress increases to a maximum value and then decreases to zero. As a result, the CP is a shear-thinning fluid where the viscosity decreases when the surrounding environment exerts shear forces. Furthermore, for a nil shear rate, the curves do not exhibit a nil shear stress. This is a typical behavior of a pseudoplastic material with yield, where a threshold must be attained before the shear stress increases with the shear rate (He *et al.* 2004). However, it was not possible to measure this threshold with the viscometer used in this research, as it does not measure shear stress for shear rates lower than 5 rpm. Linear extrapolation was used to estimate the yield stress (in yellow).At week 2, it is possible to see that the behaviour is slightly different, at zero shear stress there is a shear rate. This can be explained by the numerical errors resulting from the combined use of numerical models (linear extrapolation and cubic spline) as well as errors resulting from the machine at very low shear rate.

The yield stress, or the threshold of applied stress at which all deformation of the material becomes plastic, can be approximated using a mini slump test. As presented on Table 3.2, the yield stress is

determined to be around 2% of torque. The result is comparable for all the samples, even though the yield stress is relatively lower for week 2 than for weeks 4, 6 and 8.

Table 3. 2- CP yield stress

	Week 2	Week 4	Week 6	Week 8
Yield Stress in cP	1344.22	1386.52	1402.90	1386.52
Yield Stress in % of torque	2.02	2.09	2.11	2.09

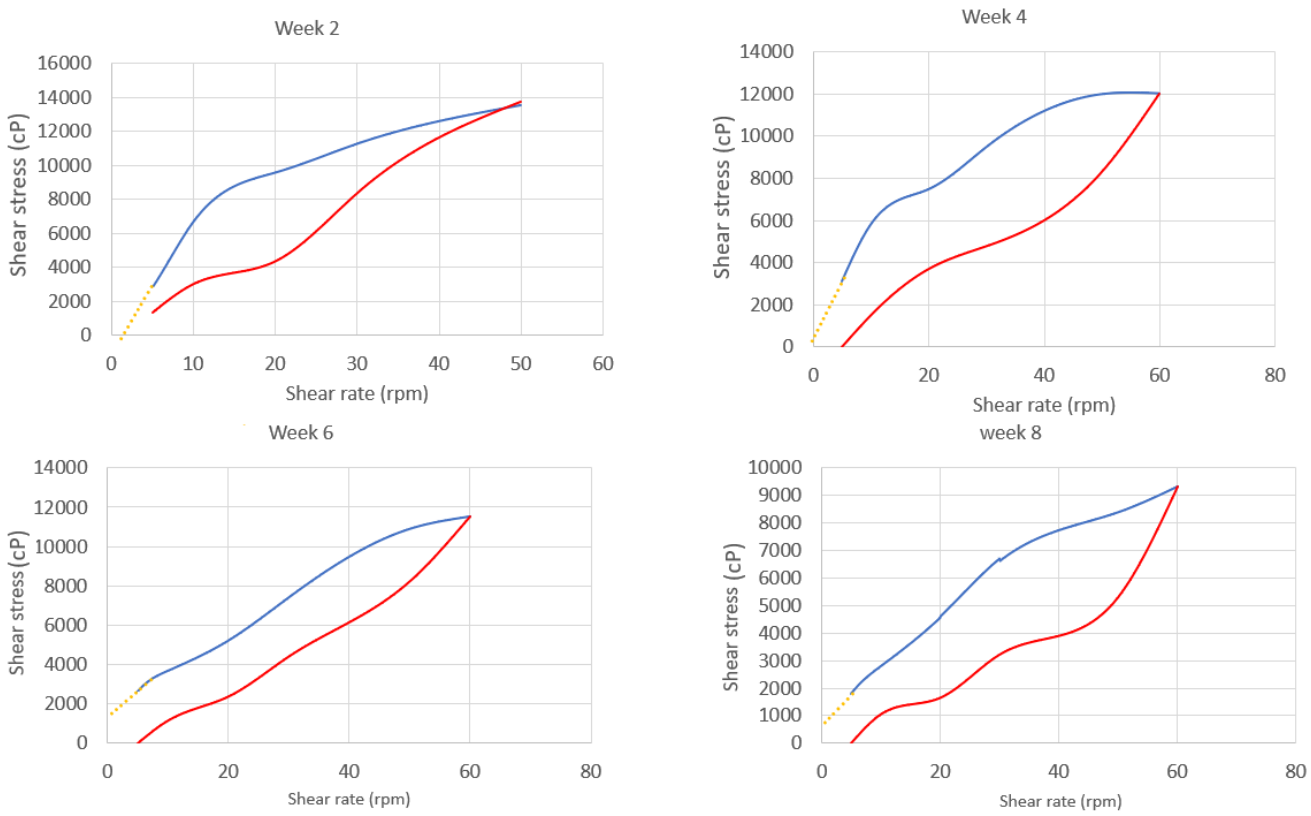

Figure 3. 12- Ascending (blue) and descending (red) measurement of shear stress vs Shear rate

The viscosity of CP at a given shear rate is represented by the slope of the ascending curve. The curve function between two points was calculated using a spline cubic, and the viscosity for that interval was found by calculating the first derivative of the same function. Figure 3.13 shows how the viscosity of CP varies with increasing shear rate for every specimen. It is observed that from 5 rpm to 20 rpm there is a drastic drop of viscosity. This can be explained by the fact that weak inter-molecular bonds such as hydrogen bonds within particles get destroyed as soon as a movement is activated in the CP and result in free particles. Following this, when the shear rate increases further,

the molecules are pushed one against each other to get rearranged and form 3D network bonds. This is demonstrated by the peak that appears between 20 and 40 rpm. After 40 rpm the viscosity drops back, once again, caused by the destruction of hydrogen bonds from the gel of molecules. At 60 rpm the viscosity of the CP hits a plateau and is almost nil.

CP's viscosity at week 2 is much higher than the other samples from 0 to 20 rpm. This is caused by the difference in particle size. The bigger the particle size the higher the viscosity, and the higher the drop in viscosity. Nevertheless, at higher torque regimes, the plots for all weeks are close to each other.

The change in viscosity when the shear rate increases for week 6 and 8 samples happens earlier when for week 2 and 4 samples. As the particles are smaller for week 6 and 8, it is easier to break the inter-molecular bonds. As a result, the shear-thining behaviour of CP is more evident as its particles get smaller in size.

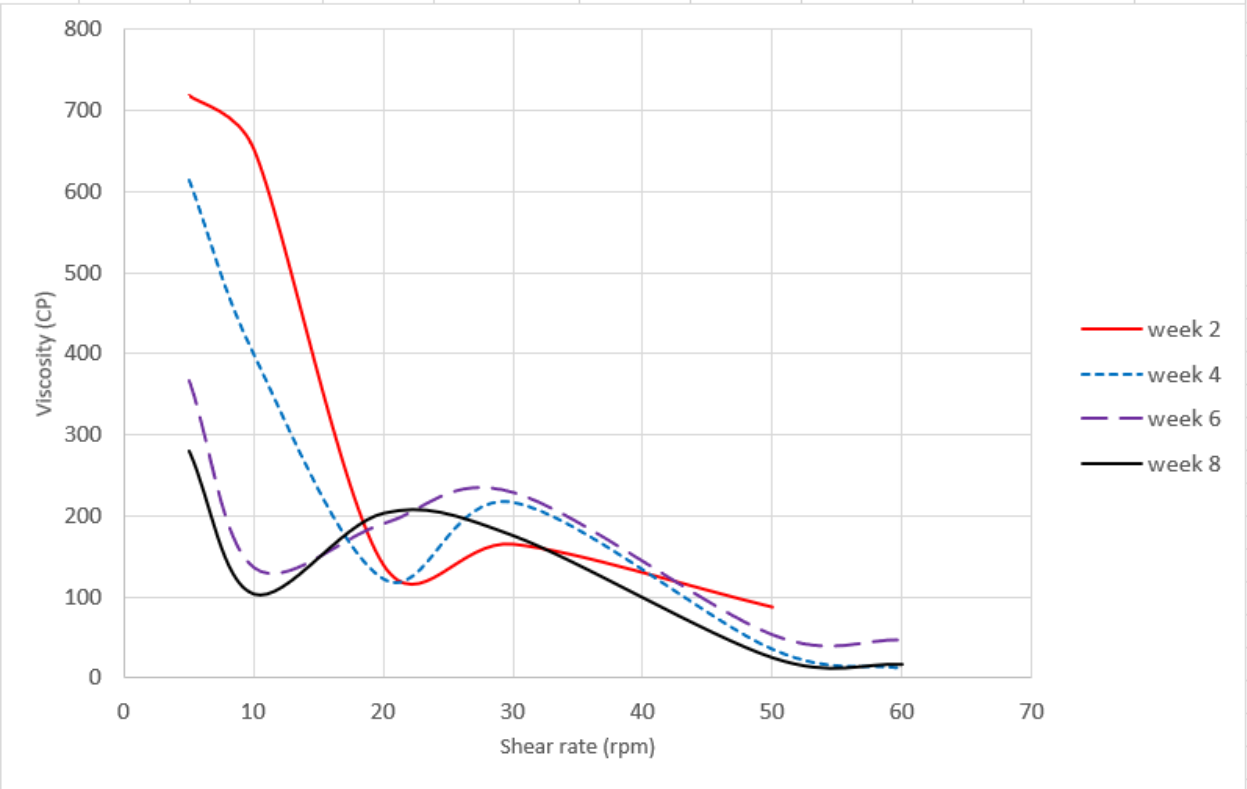

Figure 3. 13- Viscosity of CP with increasing shear rate

3.5.4 Physical Properties

During the oxidization process of corrosion, the physical properties of CP change. The density of each oxide phase is different and decreases with time. When corrosion occurs in RC, the iron oxides have a lower density, consequently increasing their volume. The density of CP is inversely proportional to its volume.

The CP density measured in this research is presented in Figure 3.13. The data show that there is a decrease of 2981 kg/m^3 in density within 2 weeks of accelerated corrosion. At the 2nd week, the majority of the CP can be identified as magnetite. However, from week 2 to week 4, there is an increase of density; the density is similar to the theoretical density of hematite. At week 6, the dominant oxide was found to be goethite, and at week 8, lepidocrocite. The results prove that at each stage of corrosion the physical properties of CP change. Hence, it is possible to use the density of CP to determine its oxidation level.

In addition, the variation in density from one sample to the next is not consistent. For the week 4 sample, the density increased. However, the density keeps on dropping after week 4. Moreover, the highest variation is noticed between week 0 and week 2. This means that there is a high level of chemical reactions that occur during this period. The first two weeks of corrosion is when the geometrical parameters of the hydrogen bonds help to decompose the iron oxide particles (Umeyama and Morokuma 1976). From week 2 to week 4, there is formation and reorganization of particles networks; during this stage element bonds are hard to break, so the chemical reactions are limited. For this reason, the variation of density is low between week 2 and week 4. After forming particle networks, the elements get rearranged and hydrogen bonds can decompose the particles once again. Table 3.3 tabulates the variation of CP density with time. These data were collected by averaging the density measurements of 10 samples from each week. As seen in Table 3.3, the variation of density increases between week 4 and week 6. Finally, there is formation and rearrangement of particle networks once again at week 8, where the variation in density and the density itself are the lowest.

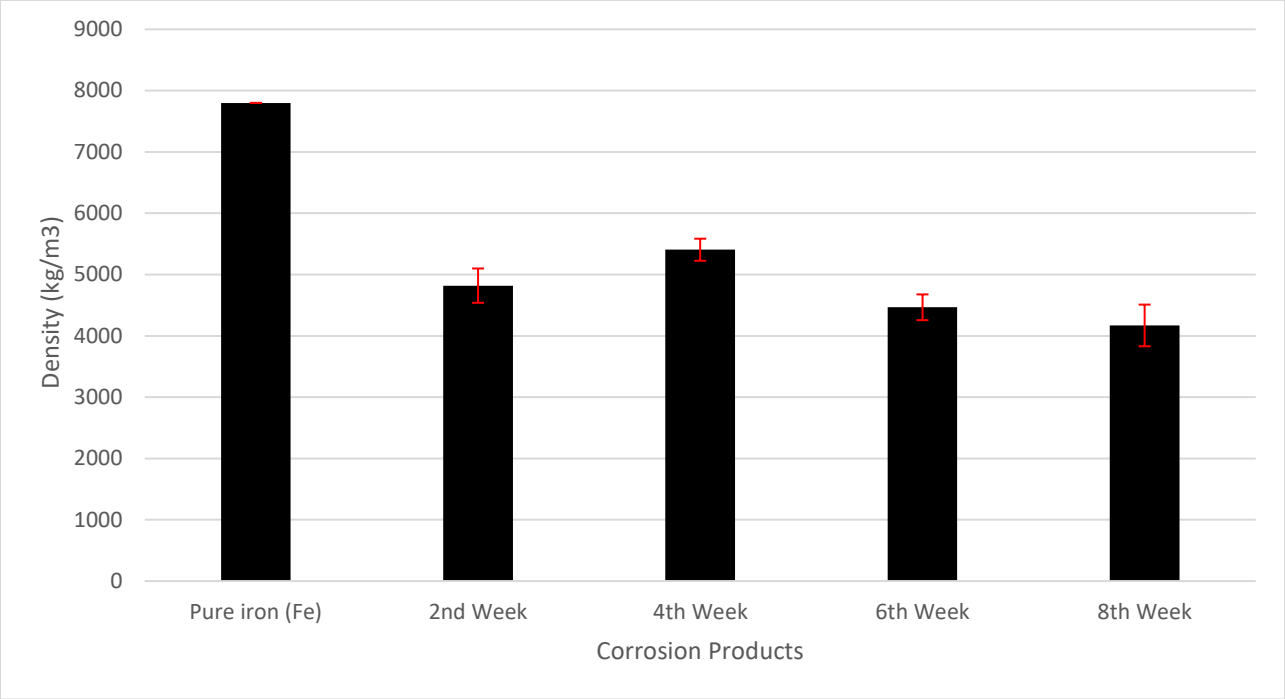

Figure 3. 14- Density of CP with time

Table 3. 3- Variation of CP density with time

Sample	Density (kg/m^3)	Associated oxide
Pure iron (Fe)	7800	Iron
2^{nd} Week	4819	Magnetite
4^{th} Week	5405	Hematite
6^{th} Week	4466	Goethite
8^{th} Week	4170	Lepidocrocite

3.6 Conclusions

The research aimed to characterize and understand the behavior of corrosion products in RC structures. The rheological behavior of the CP product was determined using methods such as

XRD, SEM, density test, viscosity test, particle size analysis and rheology test. The main findings of the current research are presented below:

- Goethite, magnetite and lepidocrocite are the three most dominant oxides present in the CP obtained by oxidizing pure iron. They are found in all the samples from the 2nd week to the 8th week of accelerated corrosion. The most dominant oxide is magnetite which is present throughout the whole corrosion process up to the 8th week. As the electrochemical reaction progress in the corrosion process, the amount of pure iron in the CP decreases with time.
- The SEM micrographs confirm the presence of goethite, magnetite and lepidocrocite at every stage of the corrosion process. However, it is possible to see that the particle size and distribution and morphology in the CP is variant at every stage.
- The change in particle size during the corrosion process is indicative of the electrochemical reactions beget degradation of elements. This is also proven by the variation of the CP density between the samples.
- Corrosion products are pseudoplastic pastes with yield; they behave as a colloidal material. Because the viscosity of CP (paste) decreases when the shear rate increases, CP can be identified as a shear-thinning material. This being said, the rheological behavior of CP at each stage is different.

3.7 References

Andrade, C. (2013). "Oxide formation due to rebar corrosion and its relation to cover cracking." 8th International Conference on Fracture Mechanics of Concrete and Concrete Structures. Post Conference Workshop - 14 March 2013

Andrade, C, and C Alonso. 2001. “On-Site Measurements of Corrosion Rate of Reinforcements.” Construction and Building Materials 15: 141–45.

Antunes, Renato Altobelli, Isolda Costa, Dalva Lúcia, and Araújo De Faria. 2003. “Characterization of Corrosion Products Formed on Steels in the First Months of Atmospheric Exposure 403 Characterization of Corrosion Products Formed on Steels in the First Months of Atmospheric Exposure.” *Materials Research*. Vol. 6.

Bohloli, B., and C. J. de Pater. 2006. “Experimental Study on Hydraulic Fracturing of Soft Rocks: Influence of Fluid Rheology and Confining Stress.” *Journal of Petroleum Science and Engineering* 53 (1–2): 1–12. https://doi.org/10.1016/j.petrol.2006.01.009.

Gotić, Marijan, and Svetozar Musić. 2007. “Mössbauer, FT-IR and FE SEM Investigation of Iron Oxides Precipitated from FeSO4 Solutions.” *Journal of Molecular Structure* 834–836 (SPEC. ISS.): 445–53. https://doi.org/10.1016/j.molstruc.2006.10.059.

Greenwood, R, N Rowson, S Kingman, and G Brown. 2002. “A New Method for Determining the Optimum Dispersant Concentration in Aqueous Grinding.” *Powder Technology* 123: 199–207. www.elsevier.comrlocaterpowtec.

He, Mingzhao, Yanmin Wang, and Eric Forssberg. 2004. “Slurry Rheology in Wet Ultrafine Grinding of Industrial Minerals: A Review.” *Powder Technology* 147 (1–3): 94–112. https://doi.org/10.1016/j.powtec.2004.09.032.

Leong, Yee-Kwong, Peter J Scales, Thomas W Healy, and David V Boger. 1995. “Effect of Particle Size on Colloidal Zirconia Rheology at the Lsoelectric Point.” *Am. Ceram. SOC.* Vol. 78.

Lundgren, Karin. 2002. “A Model for the Bond Between Corroded Reinforcement and Concrete.” Chalmers University of Technology.

Molina, F J, C Alonso, and C Andrade. 1993. “Cover Cracking as a Function of Rebar Corrosion: Part 2 Numerical Model.” *Materials and Structures* 26: 532–48.

Oh, Sei J., D.C. Cook, and H.E. Townsend. 1998. “Characterization Of Iron Oxides Commonly Formed As Corrosion Products On Steel.” https://doi.org/10.1023/A:1011076308501.

Ouglova, A., Y. Berthaud, M. François, and F. Foct. 2006. “Mechanical Properties of an Iron Oxide Formed by Corrosion in Reinforced Concrete Structures.” *Corrosion Science* 48 (12): 3988–4000. https://doi.org/10.1016/j.corsci.2006.03.007.

Robotti, Nadia. 2013. “The Discovery of X-Ray Diffraction.” In *Rendiconti Lincei*. Vol. 24. https://doi.org/10.1007/s12210-012-0205-1.

Tan, Zhijun, Susan A. Bernal, and John L. Provis. 2017. “Reproducible Mini-Slump Test Procedure for Measuring the Yield Stress of Cementitious Pastes.” *Materials and Structures/Materiaux et Constructions* 50 (6): 1–12. https://doi.org/10.1617/s11527-017-1103-x.

Tilly, Graham. 2007. “The Durability of Repaired Concrete Structures.,” 1–8. https://doi.org/10.2749/222137807796120030.

Umeyama, Hideaki, and Keiji Morokuma. 1976. “The Origin of Hydrogen Bonding. An Energy Decomposition Study.” *American Chemical Society* 99 (5): 1316–31. https://pubs.acs.org/sharingguidelines.

Verma, Amit, Geetanjali Chauhan, Partha Pratim Baruah, and Keka Ojha. 2018. “Morphology, Rheology, and Kinetics of Nanosilica Stabilized Gelled Foam Fluid for Hydraulic Fracturing Application.” *Industrial and Engineering Chemistry Research* 57 (40): 13449–62. https://doi.org/10.1021/acs.iecr.8b04044.

Wrobel, Michal, Gennady Mishuris, and Panos Papanastasiou. 2021. “On the Influence of Fluid Rheology on Hydraulic Fracture.” *International Journal of Engineering Science* 158. https://doi.org/10.1016/j.ijengsci.2020.103426.

Zhang, Weiping, Junyu Chen, and Xujiang Luo. 2019. “Effects of Impressed Current Density on Corrosion Induced Cracking of Concrete Cover.” *Construction and Building Materials* 204 (April): 213–23. https://doi.org/10.1016/j.conbuildmat.2019.01.230.

Chapter 4

4. Distribution and migration of corrosion products in cement paste

4.1 Abstract

This chapter aims to determine a correlation between the rheological behavior of corrosion products (CP) and the formation of corrosion-induced cracks in reinforced concrete. Moreover, the progress of the distribution and migration of CP through different geometries of cracks is evaluated. Reinforced cement paste samples with 0.35, 0.4, and 0.5 w/c ratio were subject to an impressed current density for 2, 4, 6 and 8 weeks. Microscopic assessments were used to characterize the elemental composition, distribution, and migration of CP as well as the geometry and crack density of the corrosion driven cracks. The results show that the distribution of CP is not uniform around the rebars. In addition, the cement paste damage caused by CP depends on the w/c ratio of the cement paste mix and the exposure time to a corroding environment. The rebar mass results show that CP is formed layer by layer. Hence, the flow of each CP layer can differ.

4.2 Introduction

Reinforced concrete (RC) is the most used construction material in the world (Song and Saraswathy 2007). However, RC can undergo deterioration caused by mechanisms such as reinforcement corrosion, freeze and thaw, alkali aggregate reactions, and many more. Corrosion of reinforcing steel is the most common and recurring problem in RC structures (Tilly 2007). Type GU concrete with a pH of 13 provides a naturally protective environment for steel reinforcing bars (Bertolini 2008). However, in the presence of chloride ions or carbonation of the concrete cover, the passive film of the reinforcement is broken, leading to the onset of reinforcement corrosion. At this stage, an expansive layer of corrosion products (CP) is developed, covering the surface of the reinforcing bars and reducing their cross-sectional area. The CP is generally

composed of 3 iron oxide phases: magnetite, goethite and lepidocrocite (Gotić and Musić 2007). The concrete cover is subjected to internal tensile stresses caused by the hydraulic pressure induced by the accumulation of the CP. When the tensile capacity of the concrete cover is reached, micro fractures start to appear in the concrete, growing into a network of cracks extending from the steels rebars to the outer surface of the concrete. This phenomenon is also known as the hydraulic fracturing process, where the CP acts as the fracturing fluid (Wrobel *et al.* 2021). The progress of the formation of CP and ensuing concrete cracks is shown in Figure 4.1.

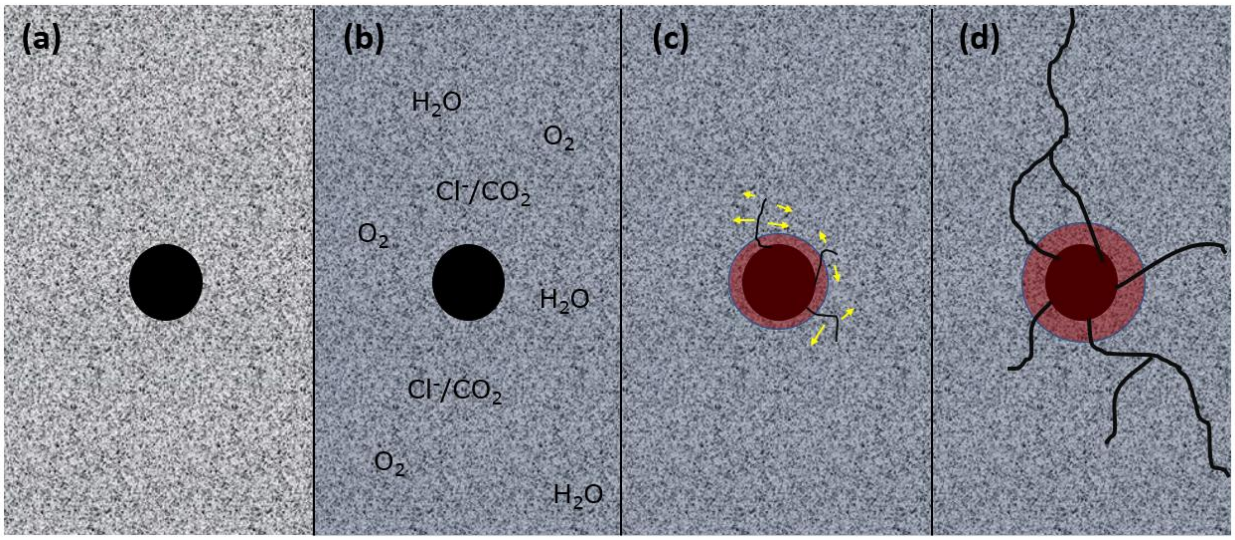

Figure 4. 1- (a) Undamaged reinforced concrete (b) Penetration of agents in RC (c) Formation of CP and tensile stresses (d) Corrosion-induced cracks

Figure 4. 1(a) illustrates an undamaged reinforced concrete sample. The penetration of chloride ions and/or carbon dioxide along with water and oxygen is shown in Figure 4. 1(b). When reinforcing steel is depassivated, CP is formed around the rebars as seen on Figure 4. 1(c). The build-up of CP exerts a pressure against the surrounding concrete, initiating micro cracks when the tensile strength of the concrete is exceeded. The internal tensile stresses are represented by arrows. As CP forms and accumulates over time, it flows through the cracks and acts as a fracturing fluid, propagating the cracks and making them larger in width. Eventually, when the cracks surpass a certain critical length, they extend from the rebars to the outer surface of the concrete creating a network of cracks as seen in Figure 4. 1(d).

The number and width of cracks created through the corrosion process are a function of the corrosion rate, the type of CP and the water-to-cement ratio of the concrete matrix, which dictates

the porosity and tensile strength of the concrete cover. Hence, the study of CP in parallel to the study of corrosion driven cracks is crucial to understand the mechanical damages caused by reinforcement corrosion in RC.

4.3 Background

The corrosion process is triggered when chloride ions (or CO_2 molecules) travel from the outside environment to the reinforcement through the concrete cover and depassivate the reinforcing steel. This process is affected by several factors, one of them being the thickness of the concrete cover. Regulations regarding concrete covers are presented in concrete standards, such as CSA A23.1-14 Table 17. Depending on the type of structure and environmental surroundings, specific concrete cover dimensions must be adopted (CSA A23.1-14 2014). In addition to this, the permeability of concrete, the water-to-cement ratio, the alkalinity and the amount of chloride ions present are aspects that can influence the timing, type and result of the corrosion process. The porosity of concrete is directly related to the water-to-cement ratio of concrete. The Canadian Standard Association (CSA A23.1-14/A23.1-14) specifies the maximum water-to-cement ratio of a concrete mix depending on the environmental conditions (CSA A23.1-14 2014). Chen *et al.* related the water-to-cement ratio of a concrete mix to the pore diameter and the cumulative intruded pore volume (Chen and Wu 2013).

Corrosion-induced cracks are a result of the different parameters cited above. However, one of the main factors that influences the cracking of concrete exposed to corrosion is the distribution and flow of the CP. The distribution of CP around rebars is difficult to determine; almost all modelling attempts and studies have been based on the assumption that corrosion products are distributed uniformly (Keivan and Hossein 2011; Roshan 2017; Molina *et al.* 1993; Balafas and Burgoyne 2011). Studies have shown that the CP deposits on the reinforcing steel gradually in layers, increasing the rust thickness around the rebar (Suda *et al.* 1993). Once concrete cracking occurs, the propagation and transport of CP through the cracks progresses. As assumed by Keivan and Hossein (Keivan and Hossein 2011), in a porous reinforced concrete sample, CP migrates through the pores and micro cracks of concrete towards the outside of the concrete cover to become visible. The rust is brought to the surface of the concrete cover by a convection and diffusion process that creates movement (Keivan and Hossein 2011).

The interaction between a non-Newtonian fracturing fluid such as the CP and a porous media is highly complex, especially because multiple parameters can govern the penetration and flow of the fluid. The rheological characteristics of CP should be studied in depth to understand its behavior in RC.

4.4 Scope of the Work

Some works have previously evaluated the distribution and propagation of CP around the reinforcing bars (Suda *et al.* 1993; Keivan and Hossein 2011; Zhao *et al*. 2012; Apostolopoulos *et al.* 2019). However, very few have addressed the influence of the rheological behavior of the CP, a fracturing fluid, on the development of cracks. The purpose of this study is to determine a correlation between the CP's properties with its distribution and migration through corrosion-induced cracks. These parameters can be determined by doing microscopic assessments on corroded reinforced cement paste samples. Rebar gravimetric mass loss and crack density are evaluated to better understand hydraulic-induced fracturing driven by the CP in RC.

4.5 Materials and Methods

The experimental procedure included 3 phases: (1) Phase I consisted of casting and mounting reinforced cement paste samples with different w/c ratios; (2) Phase II was dedicated to applying an accelerated corrosion regime to the samples for a period of 8 weeks; and, (3) Phase III focused on the microscopic assessment of the samples and ensuing corrosion-induced damage. In a separate setup, steel reinforcing wires were subjected to an accelerated corrosive and alkaline environment for 2, 4, 6 and 8 weeks. These wires were used to measure the mass loss due to corrosion and calculate their corrosion rate following the ASTM G1-03 guidelines. The experimental details of each phase are given below.

4.5.1 Sample Preparation

Reinforced cement paste cylinders of 2.54 cm (1 inch) in diameter and 2.54 cm in height were cast. The cement paste mix was prepared using a general use (GU) Portland cement, with 2% of sodium chloride and water. In general, for reinforced concrete structures exposed to chlorides, a w/c ratio

of 0.4 is used (CSA A23.1-14 2014). The setup for this experiment is also exposed to chlorides; hence, samples with w/c = 0.4 were used as control samples and comparatively, samples with w/c = 0.35 and w/c = 0.5 were also tested. In total thirteen cylinders with three w/c ratios were taken into consideration as seen on Table 4.1. A 1.5-mm diameter 304 galvanized steel wire placed in the centerline of the cylinder was used as reinforcement. Galvanized steel was used to fulfill the size specifications of the bars. In order to remove the Zn coating of the wires and make them more susceptible to corrosion, they were sanded 3 times with 60, 80 and 100 coarse sandpapers until there was not residue of coating as verified by an XRD test.

Table 4. 1- Table 1- Sample identification table

w/c ratio	Time of corrosion regime (weeks)	Sample name
0.35	2	0.35-2
	4	0.35-4
	6	0.35-6
	8	0.35-8
0.4	0	0.4-0
	2	0.4-2
	4	0.4-4
	6	0.4-6
	8	0.4-8
0.5	2	0.5-2
	4	0.5-4
	6	0.5-6
	8	0.5-8

The samples were left to cure on a rack above a container filled with water and sealed with a plastic cover to avoid any shrinkage damage on the cement paste. The samples were cured for 28 days, after which they were subjected to an accelerated corrosion regime. They were then cut right after being mounted with epoxy resin. The cross-sectional view of the samples is presented in Figure 4. 2 (b).

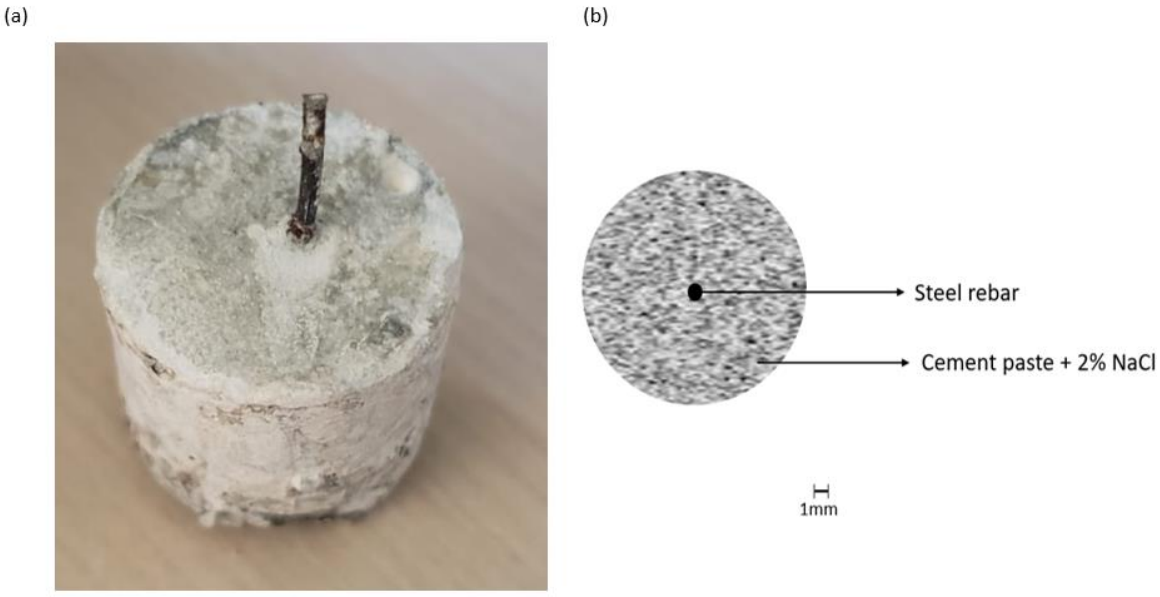

Figure 4. 2- (a) Reinforced cement paste sample (b) Cross-sectional view of a reinforced cement paste sample-

4.5.2 Accelerated Corrosion

The reinforced cement paste samples were corroded by impressing a current in the reinforcing wire. An electrical circuit was created, in which the steel wires acted as anodes. Stainless-steel tubes were placed on the outside of the cylinder to act as cathodes. To increase the electrical contact between the stainless-steel plate and the cement paste, a sponge soaked in a salt electrolyte (3.5% of NaCl) was placed in between the two as shown in Figure 4.3. The humidity conditions within the experimental setup were controlled throughout the entire duration of the process in order to keep the reinforced cement paste's resistivity stable. To induce corrosion rates representative of field conditions, researchers have noted that the current density in the circuit must be less than 1 $\mu A/cm^2$ (Andrade and Alonso 2001). A 9-volt battery with an 8.2M Ohm resistor was used to regulate and keep the current density at 0.96 $\mu A/cm^2$. The voltage was measured at different points of the voltage to assure that the calculated value of the current density stayed constant and less than 1 $\mu A/cm^2$.

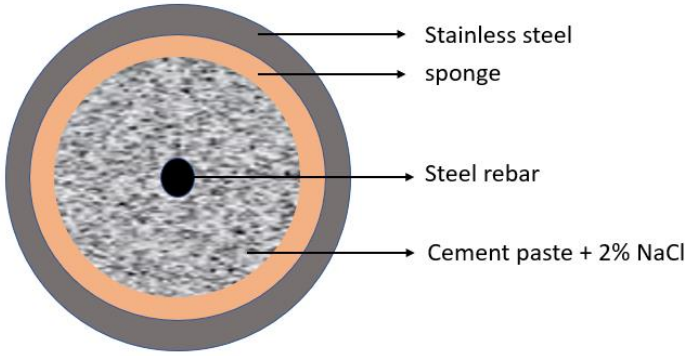

Figure 4. 3- Cross-sectional view of cement paste samples for accelerated corrosion

The accelerated corrosion regime was applied to 3 samples simultaneously for each w/c. For each batch of different w/c ratio, one sample was corroded for 2, 4, 6 and 8 weeks (4 sets of circuit). One cylinder was kept outside the corroding environment to serve as a control sample. The experimental setup of the accelerated corrosion is presented in Figure 4.4.

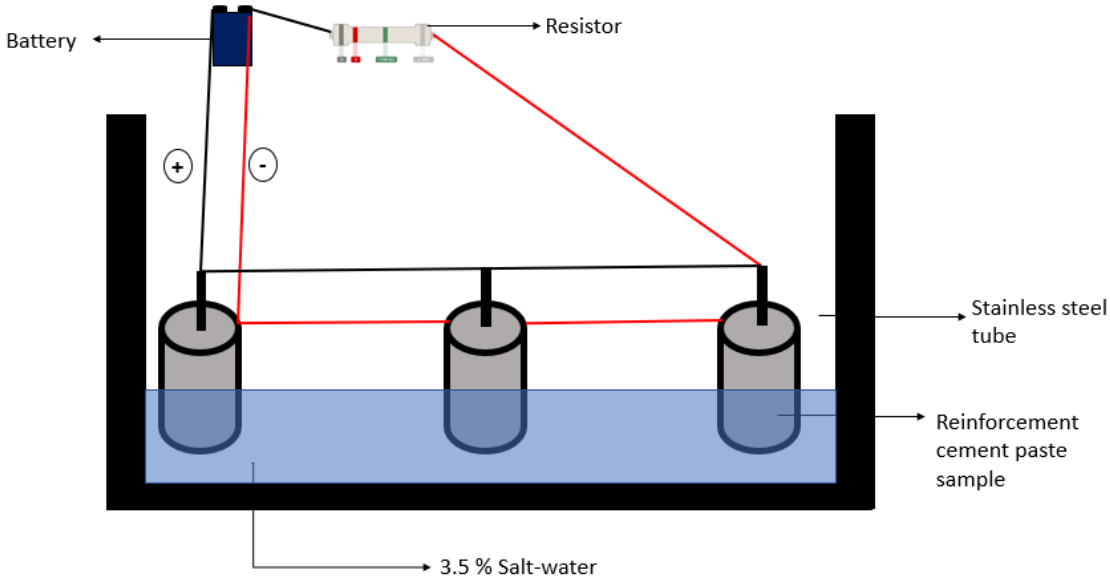

Figure 4. 4- Experimental setup for accelerated corrosion

Following the accelerated corrosion process, the samples were mounted in a Cast N' Vac 1000 Vacuum impregnation system using a EpoFix epoxy resin from Struers to stagnate the development of pores or cracks in the cement paste cover. Once the mounting had hardened overnight, the samples were cut transversally and longitudinally along the rebar axis using a 15HC

IsoMet diamond blade. Before doing any microscopic assessment, the cut samples were polished using a mechanical polish table with polishing pads MD- Molto, MD- Largo, Mol, and OP- S. The liquid solutions that were used were water, diamond solutions (for 2 pads) and colloidal silica. The polishing was repeated until a reflective surface was obtained.

4.5.3 Characterization Methods

Stereomicroscopy Analysis

Microscopic assessment of crack patterns was performed using a Zeiss STEMI 508 Greenough stereo optical microscope. The images were captured at a magnification of 16X. The number, length and orientation of cracks were analysed using these microscopic images.

Scanning Electron Microscopy

The Scanning electron microscopy with Energy dispersive spectroscopy mapping, SEM-EDS (JSM -7500F FESEM) was carried out to study the elemental composition of the cement paste samples. Eight sites of interest were selected to be traced at a magnification of 250X. The selected sites were focused around the zones with cracks and across the rebar. At the sites of interest, the following elements were mapped: Fe, O and Zn. The micrographs are represented in a gray scale; the lighter colors indicate the presence of the corresponding element.

Image J

Image J is a software used for image analysis. The length of the cracks in the samples were measured using Image J. The scale of the images was reset on the software before the measurements were taken. The results are obtained by tracing each crack all along their length in millimeters with an accuracy of 3 significant digits. In order to increase the precision of the results, the measurements were taken 3 times for each crack.

4.5.4 Gravimetric Mass Loss

Gravimetric mass loss was used to calculate the corrosion rate of steel wires. Steel wires of 25.4-cm (10 inches) in length and 2.54 cm in diameter were left in a solution of distilled water, 0.5M sodium chloride and saturated calcium hydroxide for 2, 4, 6, and 8 weeks. These conditions were set in a way to replicate the same corroding environment of a wire embedded in cement paste.

ASTM G1-03 provides a procedure to remove the CP from a corroded steel rebar without the removal of the base metal and therefore evaluate the mass loss due to corrosion (ASTM 1985). The wires were then abraded with sandpaper, rinsed and hot air dried. The mass and length were measured before and after cleaning each wire. The cleaning process was repeated until there was no increase in mass loss (ASTM 1985).

4.6 Results and Discussion

4.6.1 Corrosion Products Distribution and Migration

Corrosion-induced concrete cracks have varying orientation and geometry. A concrete crack can be characterized in different ways; however, there are no guidelines to qualify it. Nevertheless, the length, width and depth of concrete cracks are generally studied to determine the limit beyond which the permeability of the material is affected (Wang *et al.* 2016). Thirteen samples were studied in total, with 3 different w/c ratios: 0.35, 0.4, and 0.5. The development of cracks determines if there is a correlation between the w/c ratio and the crack geometry and CP distribution.

The cracking pattern of the reinforced cement paste samples and the distribution of CP was first assessed by visual inspection. Table 4.2 presents a summary of the visual observations from the samples with w/c = 0.4. A complete summary of all the transversal cuts of all samples is presented in Table B.1 and Table B.2 in the Appendix. The control sample with no corrosion showed no trace of CP and no corrosion-induced cracks. At week 2, the samples exhibited the presence of CP. The products are seen around the wires and are not uniformly distributed. After 4 weeks of accelerated corrosion, it is possible to see that the CP has spread and started to fill out the voids around the rebar. For week 6 and week 8, the same trend is followed; more CP is dispersed throughout the cement paste cover, penetrating and filling more of the pores around the steel rebar. At week 8, clumps of CP are concentrated at specific regions on the exposed surface of the steel. Similar observations were reported by Zhao *et al.* who noted that the stage when expansive pressure is exerted by the fracturing fluid and the stage when the CP fills all the porous zones are not dependent and can take place simultaneously (Zhao *et al*. 2012).

Table 4. 2- Visual inspection of cement paste samples with w/c = 0.4

Duration of accelerated corrosion	Observations	Image
0.4-0	• No crack	
0.4-2	• 1 corrosion-induced crack • The crack starts at the rebar and extends to the outer surface of the sample. • Only the wider section of the crack is filled with CP • CP is not uniformly distributed around wire • CP fills the voids around the wire	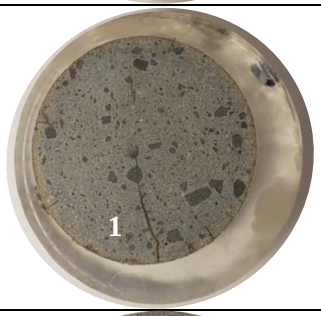
0.4-4	• No corrosion-induced cracks • CP covers the whole perimeter of the wire • CP is not uniformly distributed around the wire	
0.4-6	• 2 corrosion-induced cracks • one of the cracks extends from the wire all the way to the outer surface while the other one stops halfway. The third crack originates from the outer surface of the cement paste • The cracks at the wire are filled with CP • CP is not uniformly distributed around the wire • More CP is found close to pores and cracks	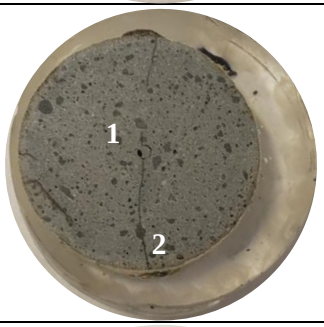
0.4-8	• 1 corrosion-induced crack + multiple shrinkage cracks • one crack that goes from the wire to the outer surface of the sample • small shrinkage cracks are present around the surface perimeter • CP is not uniformly distributed around the wire • Stains of CP are seen on the surface of the wire • More CP is concentrated close to the crack	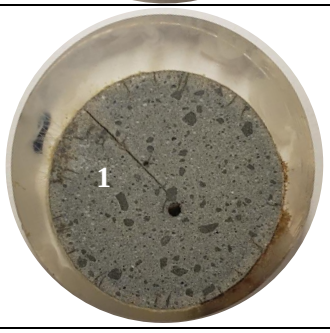

The CP analysis was conducted on longitudinal cuts of the samples as well. It can be noticed that the CP is more concentrated on the side of the samples that was exposed to moisture during the accelerated corrosion process. This shows that the CP flows differently where moisture is present. At week 2, the CP has contoured the perimeter of the steel rebar. Figure 4. 5- Longitudinal cut of reinforced cement paste (w/c=0.4) sample after 8 weeks of accelerated corrosion shows a longitudinal cut of a reinforced cement paste sample (w/c = 0.4) after 8 weeks of accelerated corrosion. The CP is not uniformly distributed around the rebar, it is mostly concentrated on the side that was exposed to water during the accelerated corrosion process and all around the rebar. The flow of CP is not linear or does not follow a specific pattern; it seems like it travels through the concrete cover by filling out each adjacent pore. After 8 weeks of accelerated corrosion, CP traveled approximately 5 mm to each side of the wire on the side that was exposed to moisture, but only 2 mm on the side that was not exposed to moisture. This proves the fact that CP is a colloidal fluid that follows the flow of the fluid that it encounters on its path. In Table B.1, the samples that were cut longitudinally after 2, 4, 6, or 8 weeks of accelerated corrosion (0.4-2(L), 0.4-4(L), 0.4-6(L) and 0.4-8(L)) exhibit the same pattern of CP spread. These images show that the CP fills all the pores around the rebar first (2 weeks). With time, the CP migrates to neighboring pores starting from the side that is exposed to water (4 weeks). Finally, the products make their way through the cracks from the surface of the rebar (6 and 8 weeks).

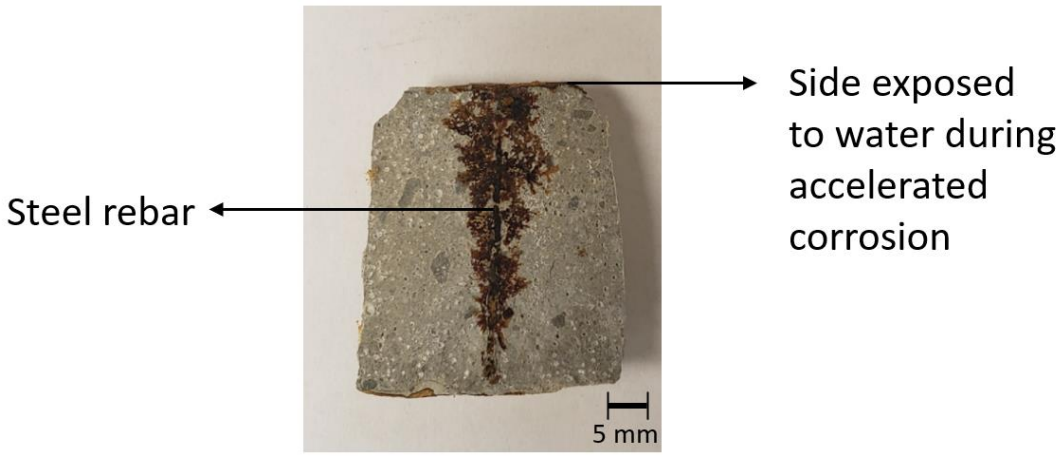

Figure 4. 5- Longitudinal cut of reinforced cement paste (w/c=0.4) sample after 8 weeks of accelerated corrosion

To further understand the flow of CP, EDS mapping was conducted for all samples of w/c = 0.4 with no corrosion and 2,4, 6, and 8 weeks of accelerated corrosion, as illustrated in Table 4.3. The sample that was not exposed to corrosion does not show any trace of iron or oxygen other than iron for the steel itself. This proves that if the corrosion process is not accelerated, the electrochemical reactions do not take place right away at any region of the sample. At week 2, the presence of iron oxide can be seen at the interfacial transition zone (ITZ) between the cement paste and the steel wire. However, the CP has not penetrated through the cracks. In Chapter 3, it was proven that at week 2 almost 50% of the parent iron from the wire gets transformed into magnetite. In accordance with the EDS images, it is possible to confirm that the CP present all around the wire is magnetite. At week 4, the map shows that the CP has migrated from the ITZ to the base of a crack. It can also be noticed that the concentration of iron and oxygen has increased because the electrochemical reactions of corrosion become more reactive with time. At this stage, more iron oxide phases such as goethite and lepidocrocite and formed. At week 6, the larger voids in the cement paste cover near the wire are filled with CP. The fact that more pores are filled with CP can be explained by the decrease of CP's particle size that allows its flow to be more feasible (Chapter 3). Finally, at week 8, it is possible to see that the CP has gone further into the cracks and away from the ITZ. The colors indicating the presence of the elements are more distinguished. Therefore, the concentration of these elements has increased with time and the electrochemical reactions inciting corrosion are dominant. Similarly, in Chapter 3 it was proven that at the end of week 8, magnetite, goethite and lepidocrocite dominate the chemical composition of CP.

Table 4. 3- EDS mapping (Fe and O) on reinforced cement paste samples with w/c = 0.4

Samples	Electronic image	Iron (Fe)	Oxygen (O_2)
0.4-0	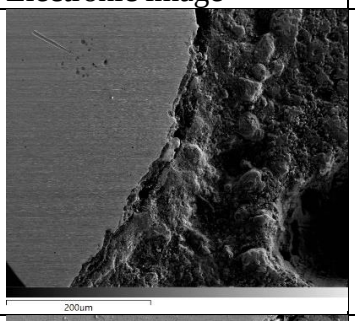	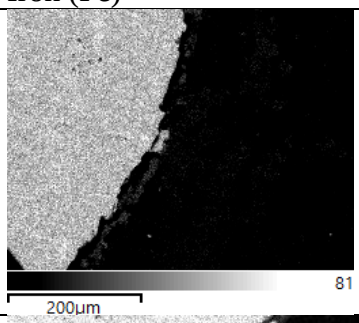	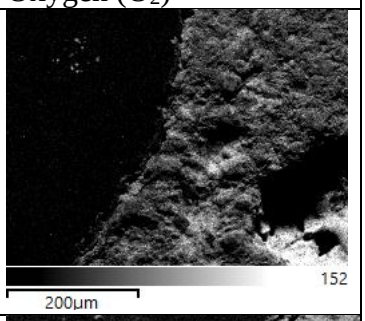
0.4-2	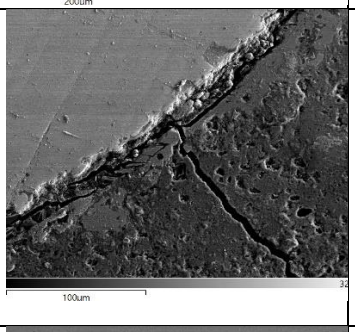	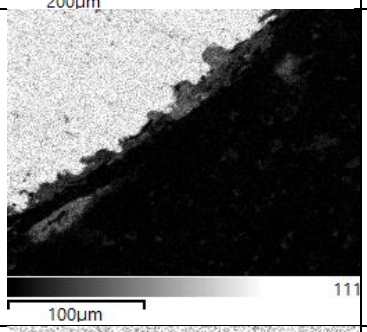	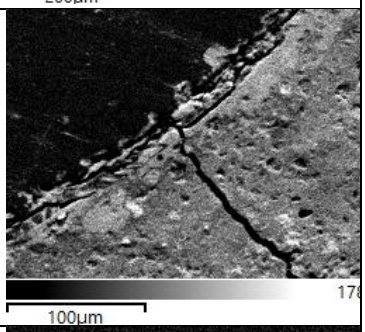
0.4-4	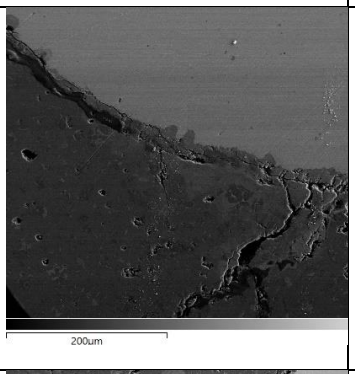	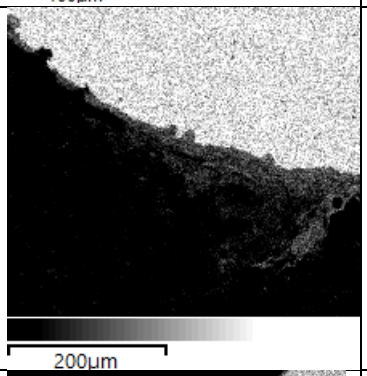	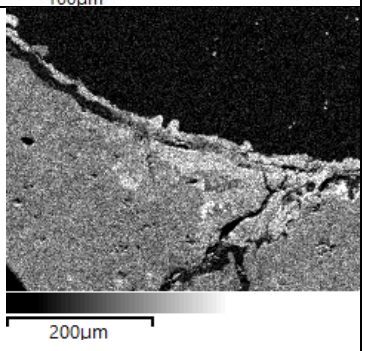
0.4-6	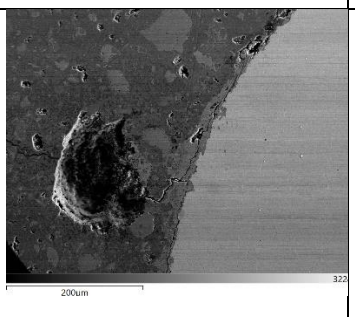	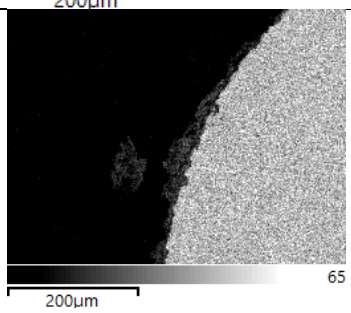	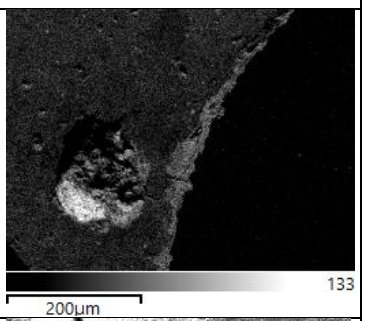
0.4-8	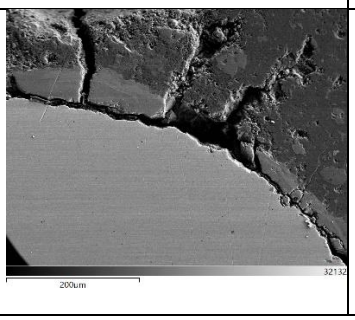	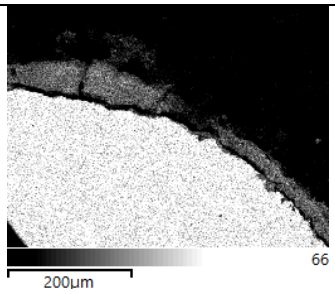	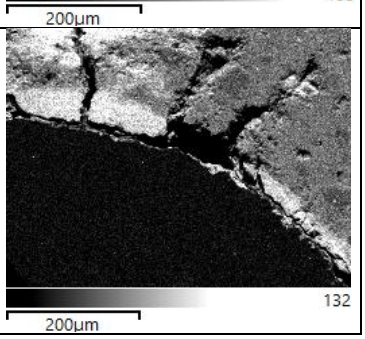

When the density of CP decreases, its volume increases and the buildup of CP gets larger with time, causing extra pressure on the surrounding cover but also on the CP itself. In Figure 3. 15 of Chapter 3, it was proven that the viscosity of CP decreases with an increasing shear rate. For this reason, at week 8, CP flows thought the cracks as it becomes less viscous.

4.6.2 Crack Analysis

To detect and quantify the crack characteristics in the reinforced cement paste, the samples were imaged with a digital camera as well as an optical microscope. Cracks that originated at the steel/cement paste interface were identified as corrosion-induced cracks. Cracks originating at the perimeter of the samples were caused by other mechanisms such as shrinkage and the sample polishing process. After 2 weeks of accelerated corrosion, only one sample of w/c = 0.4 presented a corrosion-induced crack. The samples exhibited 0 corrosion-induced cracks for 0.35 w/c ratio at week 8, and 1 corrosion-induced crack for 0.4 w/c and 0.5 w/c ratio the end of 8 week of accelerated corrosion. This shows that a concrete mix with a higher w/c ratio is more prone to have corrosion-induced cracks as the tensile strength is lower. At a lower w/c, concrete exhibits lower porosity. Table B.1 shows that in general the cracks increase in length and in number when the exposed time for accelerated corrosion is longer. All of the corrosion-induced cracks extend from the rebar to the outer surface of the cement paste sample. The cracks get wider as they approach the outer surface of the sample. Only two samples (0.35-4 and 0.35-6) formed a shrinkage-crack network. All the corrosion-induced cracks that are formed follow a straight radial line, except for the cracks in sample 0.35-6. However, since the ratio of the actual path length to the length of displacement of the cracks in sample 0.35-6 is relatively small, the tortuosity of the cracks is not taken into account in all the measurements.

Crack density is another parameter that quantifies the cracks in concrete. It is defined as the area of cracks per unit of observation area (506.7 mm^2). The formula used to calculate the crack density is given by (Nemati *et al*. 1998):

$$\rho = \frac{1}{A} \sum_{i=1}^{N} l_i^2 \qquad \textit{Eq.4.1}$$

where
ρ = crack density
l = crack length
A = material surface area
N = number of corrosion-induced cracks

The crack densities of the samples for different w/c ratios after 2, 4, 6 and 8 weeks of accelerated corrosion are presented in Figure 4.6 and Table 4. 4. The data presented in Figure 4.6 are generated from a small number of samples; hence, the results cannot be generalized. However, it is possible to see a pattern in the evolution of crack density. At week 2, the crack density is the highest for w/c = 0.4. At week 4, there were no cracks observed for w/c = 0.4. However, the crack density increases back up at week 6 and week 8. The crack density for w/c = 0.5 and 0.35 increases until week 4 and 6 respectively . The crack density at week 8 for w/c = 0.35 and 0.5 decreases.

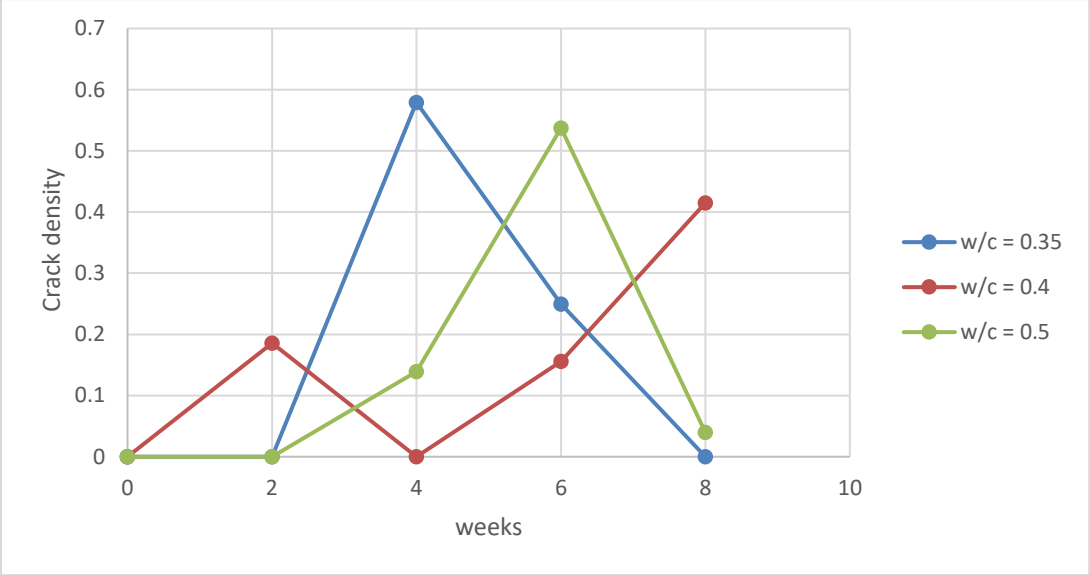

Figure 4. 6- Corrosion-induced crack density in reinforced cement paste

Table 4. 4- Crack length and crack density for each reinforced cement paste sample

samples	0.35-2	0.35-4			0.35-6		0.35-8	0.4-0	0.4-2	0.4-4	0.4-6		0.4-8	0.5-2	0.5-4		0.5-6	0.5-8
Crack length (mm)	-	7.5	9	12.5	8.8	7	-	-	9.7	-	8.7	1.8	14.5	-	8.3	1.3	16.5	4.5
Crack density	-	0.579			0.250		-	-	0.186	-	0.156		0.419	-	0.139		0.537	0.040

4.6.3 Steel Wire Mass Loss

Along with interface degradation and concrete cover cracking, corrosion causes a mass loss of reinforcement bars in RC. The mass loss of steel wires was calculated following the ASTM G1-03 guidelines (ASTM 1985). After 8 weeks of exposure to corrosion, the wires had an average of 0.13 g of mass loss, which represents approximately 5% of the total mass as seen in Figure 4.7.

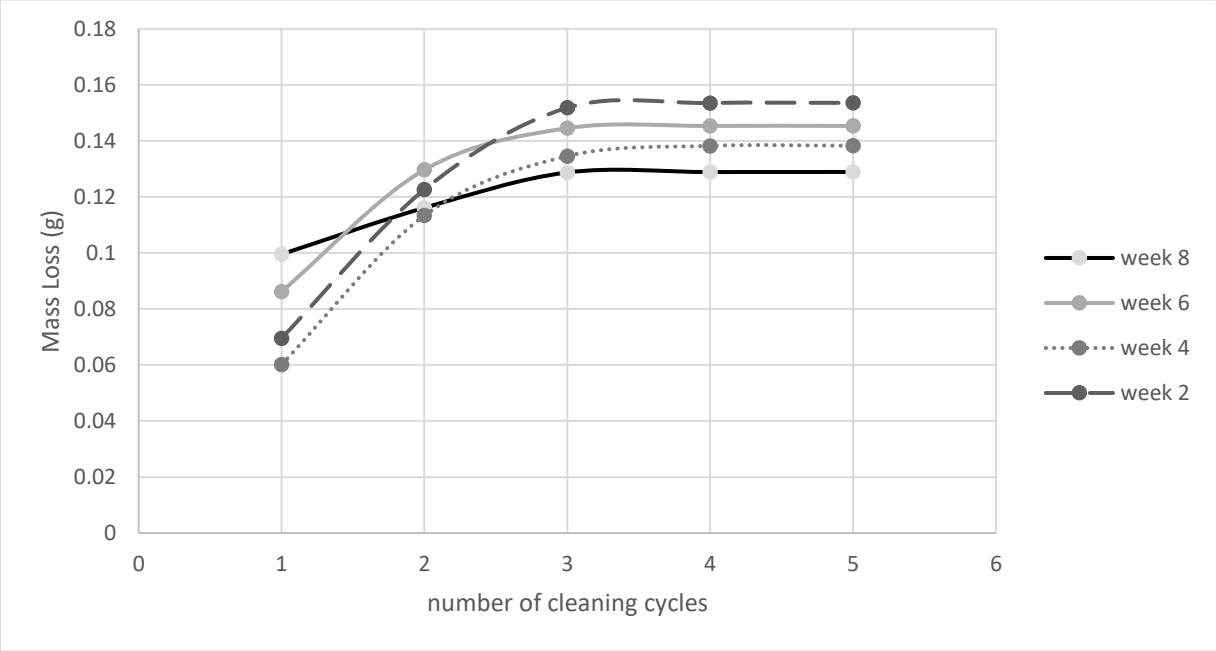

Figure 4. 7- Mass loss plot

The corrosion rate is another indicator to characterize the steel loss due to corrosion. It is calculated using the following formula (ASTM 1985):

$$Corrosion\ rate = (K * W)/(A * T * D) \qquad Eq\ 4.2$$

where

$corrosion\ rate$ = in mm/ year
K = 8.76×10^4
T = time of exposure in hours
A = area in cm^2
w = mass loss in grams
D = density in g/cm^3

Figure 4.8 presents the relationship between corrosion rate and time. It can be seen that the corrosion rate decreases with time. This is due to the fact that as the CP layer thickens, the distance between the steel wires and the cement paste increases. As a result, it is harder for moisture and oxygen to penetrate the formed CP and attain the virgin steel (Liu and Weyers 1998). As a consequence, CP is produced in layers. Therefore, the chemical composition and rheological behavior of each layer will differ. This can also explain why the distribution of CP around the rebar is not uniform as seen through the microscopic images. This concept was proven by Zhao *et al.*, where the authors observed that there are two main layers of rust that are formed around the rebars (Zhao *et al.* 2013). A thin layer of mill scale or a flaky surface iron oxide is present in contact with the steel (Zhao *et al.* 2013).

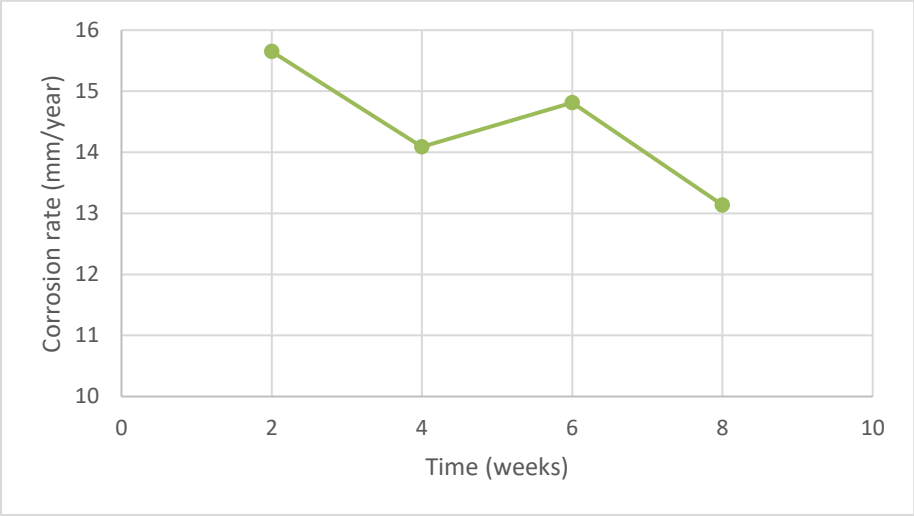

Figure 4. 8- Corrosion rate of steel wire

4.7 Conclusions

The purpose of this study was to establish a relationship between the rheological behavior of CP and the formation of corrosion-induced cracks in reinforced cement paste and to evaluate the progress of the distribution and migration of CP through cracks. The following conclusions can be drawn from the results obtained:

- The corrosion products are not uniformly distributed around the wire. The distribution of CP is done in stages. They first start by filling the space in the ITZ. They then fill out the

voids close to the reinforcing bar. Finally, they penetrate through the cracks and make their way to the center of the cement paste cover.

- The sides of the samples that were exposed to moisture were the area with the most accumulation of CP. This is can be caused by the fact that CP is suspended in a fluid and therefore moves with the flow of moisture.
- Reinforced cement paste with higher w/c ratio is more likely to have corrosion-induced cracks. The crack density of reinforced cement paste samples was found to be the highest for a cement paste mix with higher w/c ratio.
- 5% of the initial steel wire mass had been lost after 8 weeks of immersion in a corrosive environment. The corrosion rate of steel reinforcement in the cement paste samples decreases with time as there are less electrochemical reactions due to less accessibility of oxygen and water to the parent iron.

4.8 References

Andrade, C, and C Alonso. 2001. "On-Site Measurements of Corrosion Rate of Reinforcements." Construction and Building Materials 15: 141–45.

Apostolopoulos, Charis Alk, Konstantinos F. Koulouris, and Alkiviadis Ch Apostolopoulos. 2019. "Correlation of Surface Cracks of Concrete Due to Corrosion and Bond Strength (between Steel Bar and Concrete)." *Advances in Civil Engineering* 2019. https://doi.org/10.1155/2019/3438743.

ASTM. 1985. "Standard Practice for Preparing, Cleaning, and Evaluating Corrosion Test Specimens." *ASTM Special Technical Publication* i (Reapproved 2017): 505–10. https://doi.org/10.1520/G0001-03R17E01.2.

ASTM international G15 -08. 2008. "Standard Terminology Relating to Corrosion and Corrosion Testing."

Balafas, Ioannis, and Chris J. Burgoyne. 2011. "Modeling the Structural Effects of Rust in Concrete Cover." *Journal of Engineering Mechanics* 137 (3): 175–85. https://doi.org/10.1061/(ASCE)EM.1943-7889.0000215.

Bertolini, Luca. 2008. "Steel Corrosion and Service Life of Reinforced Concrete Structures." *Structure and Infrastructure Engineering* 4 (2): 123–37. https://doi.org/10.1080/15732470601155490.

Chen, Xudong, and Shenxin Wu. 2013. "Influence of Water-to-Cement Ratio and Curing Period on Pore Structure of Cement Mortar." *Construction and Building Materials* 38 (January):

804–12. https://doi.org/10.1016/j.conbuildmat.2012.09.058.

CSA A23.1-14. 2014. “Concrete Materials and Methods of Construction/ Test Methods and Standard Practices for Concrete.”

Gotić, Marijan, and Svetozar Musić. 2007. “Mössbauer, FT-IR and FE SEM Investigation of Iron Oxides Precipitated from FeSO4 Solutions.” *Journal of Molecular Structure* 834–836 (SPEC. ISS.): 445–53. https://doi.org/10.1016/j.molstruc.2006.10.059.

Keivan, Kiani, and M.Shodja Hossein. 2011. “Prediction of the Penetrated Rust into the Microcracks of Concrete Cause by Reinforcement.” *Applied Mathematical Modelling* volume 35: 2529–43.

Liu, Youping, and Richard E Weyers. 1998. “Modeling the Time-to-Corrosion Cracking in Chloride Contaminated Reinforced Concrete Structures.” *ACI Materials Journal* 95 (6): 675–81.

Molina, F J, C Alonso, and C Andrade. 1993. “Cover Cracking as a Function of Rebar Corrosion: Part 2 Numerical Model.” *Materials and Structures* 26: 532–48.

Nemati, Karman M., Paulo J.M. Monteiro, and Karen L. Scrivener. 1998. “Analysis of Compressive Stress-Induced Cracks in Concrete.” *ACI Material Journal* 60: 617–30.

Roshan, Arman. 2017. “Different Approaches to Model Cover-Cracking of RC Structures Due to Corrosion.” University of Ottawa.

Song, Ha-Won, and Velu Saraswathy. 2007. “Corrosion Monitoring of Reinforced Concrete Structures-A Review.” *Int. J. Electrochem. Sci* 2: 1–28.

Suda, Kumiko, Sudhir Misra, and Kenichi Motohashi. 1993. “Corrosion Products of Reinforcing Bars Embedded in Concrete.” *Corrosion Science* 35: 1543–49.

Tilly, Graham. 2007. “The Durability of Repaired Concrete Structures.,” 1–8. https://doi.org/10.2749/222137807796120030.

Wang, Hai Long, Jian Guo Dai, Xiao Yan Sun, and Xiao Long Zhang. 2016. “Characteristics of Concrete Cracks and Their Influence on Chloride Penetration.” *Construction and Building Materials* 107 (March): 216–25. https://doi.org/10.1016/j.conbuildmat.2016.01.002.

Wrobel, Michal, Gennady Mishuris, and Panos Papanastasiou. 2021. “On the Influence of Fluid Rheology on Hydraulic Fracture.” *International Journal of Engineering Science* 158. https://doi.org/10.1016/j.ijengsci.2020.103426.

Zhao, Yuxi, Hong Dai, and Weiliang Jin. 2012. “A Study of the Elastic Moduli of Corrosion Products Using Nano-Indentation Techniques.” *Corrosion Science* 65 (December): 163–68. https://doi.org/10.1016/j.corsci.2012.08.016.

Zhao, Yuxi, Hong Dai, Haiyang Ren, and Weiliang Jin. 2012. “Experimental Study of the Modulus of Steel Corrosion in a Concrete Port.” *Corrosion Science* 56 (March): 17–25. https://doi.org/10.1016/j.corsci.2011.11.004.

Zhao, Yuxi, Yingyao Wu, and Weiliang Jin. 2013. “Distribution of Millscale on Corroded Steel Bars and Penetration of Steel Corrosion Products in Concrete.” *Corrosion Science* 66: 160–68. https://doi.org/10.1016/j.corsci.2012.09.014.

Chapter 5

5. Concluding Remarks

5.1 Conclusions

The main purpose of this research was to characterise and appraise the rheological behavior of CP to understand and evaluate its effect on corrosion-induced cracks in RC. Previous research in this field have developed multiple experimental procedures to produce and analyze the CP. Yet, some discrepancies with regards to the results have been observed. These inconsistencies were mainly attributed to the rheological nature, distribution, flow of CP and its influence on corrosion-induced cracks in RC. In chapter 3 of this thesis, a new experimental procedure to produce CP was introduced and its nature and rheological properties studied. In chapter 4, steel reinforced cement paste samples (with different w/c ratios) were used to study the formation, distribution, and propagation of CP around the rebars and within the corrosion-induced cracks. The most important findings that were drawn from this research are presented hereafter:

- During the chloride-induced corrosion process, iron is oxidized to form different phases of iron oxide. The XRD results have proven that CP is composed of three main iron oxide phases: goethite ($Fe_3O(OH)$), magnetite (Fe_3O_4) and lepidocrocite ($FeO(OH)$). Each of these minerals have a specific morphology, density, rheological and chemical behavior. All three phases are present at every stage of corrosion process starting at the propagation stage. However, the quantitative analysis showed that at every stage the concentration of each mineral in CP is different; with that, the rheological and chemical properties of CP changed as the corrosion progresses.
- The particle size and density of CP has been proven to decrease as a function of time during the corrosion process. However, the decrease is not linear and is dependent on the dominant iron oxide phase at each stage. The particle size of the CP highly affects its rheological

behavior as the CP is a mixture of solid particles and water. The first two weeks of the process exhibit almost 50% of particle size decrease for the majority of the CP.

- The viscosity of CP decreases with an increasing shear rate; hence, CP is a non-Newtonian fluid. When the fluid is sheared harder, the less viscous it becomes, and for this reason, CP can be identified as a shear-thinning. This signifies that CP cannot be considered solely as a liquid or fine grains of iron oxide but as a colloidal material. Depending on the stage of the corrosion process, the rheological behavior of CP can differ.
- The study on steel reinforced cement paste samples have proven that CP is not uniformly distributed around the wires. The distribution of CP is done in stages. The first stage begins when CP starts filling the space in the ITZ. CP then disperses out to the voids close to the reinforcing wire. Finally, the CP penetrates through the cracks and makes its way to the outer surface of the cement paste cover. Furthermore, the sides of the samples that were exposed to moisture were the areas with the most spread of CP.
- The corrosion rate of steel reinforcement in cement paste samples decreases with time, because there are less electrochemical reactions due to less accessibility of oxygen and water to the parent iron. 5% of the initial steel wire mass had been lost after 8 weeks of immersion in an accelerated corrosive environment.

5.2 Recommendations for Future Research

Further research is however required to fully understand the rheological behavior of CP and to find all the missing properties of CP in order to feed models that simulate corrosion-induced cracking in concrete.

- As the amount of produced CP in 8 weeks was a limiting factor in the multiplicity of used characterization methods and recurrence of each tests, modifying the experimental procedure to produce CP can optimize the quality and quantity of the tests.
- As it was determined, the properties of CP at each stage are dependent on the dominant iron oxide phase at that stage. Thus, an investigation of the rheological properties of each mineral in a corrosive environment is required to better characterize the CP paste.
- Conducting Damage Rating Index (DRI) on reinforced mortar samples that are cracked will improve the assessment of corrosion-induced deterioration. The damage can be

evaluated at every point of a sample and more information on the damage generation and propagation can be obtained

- Determining the effect of the cementitious matrix, the diameter of rebar and the w/c ratio of the cover on the diameter of CP buildup can help better understand the formation and migration of CP.
- An extensive microscopic assessment on the steel reinforcement from reinforced cement paste samples can help to better correlate the rheological behavior of CP and its effect on RC and also determine the amount of CP that is produced during the corrosion process.
- Lastly, a study on the effect of other distress mechanisms such as AAR and FT on hydraulic-fracturing cracks and the mechanical behavior of reinforced concrete in accordance to the rheological behavior of CP can improve models used for structural applications. This study can be done for different stages of the corrosion process.

6. Appendices

6.1 Appendix A

Table A. 1- XRD peak identification chart for Week 2

IM-1-long-2 weeks				
Peaks	2-Theta	Intensity	Peak identified with	
1	30.22	45	Magnetite	30.2
2	35.5	166	Magnetite	35.5
3	37.48	15	Magnetite	37.5
4	43.24	31	Magnetite	43.2
5	44.78	1264	Iron- Alpha	44.8
6	57.22	40	Magnetite	57.2
7	62.84	56	Magnetite	62.7
8	65.08	147	Magnetite	65.1
9	82.4	327	Magnetite	82.3

Table A. 2- XRD peak identification chart for Week 4

IM-1-long -4 weeks				
Peaks	2-Theta	Intensity	Peak identified with	
1	14.28	62	Goethite	14.2
2	18.44	39	Magnetite	18.4
3	27.18	44	Goethite	27.1
4	29.56	151	Goethite	29.6
5	30.28	67	Magnetite	30.2
6	33.44	37	Lepidocrocite	33.4
7	35.6	243	Magnetite	35.5
8	29.6	33	Hematite	39.5
9	43.3	62	Magnetite	43.3
10	44.84	935	Iron- Alpha	44.8
11	47.86	23	Lepidocrocite	47
12	48.68	24	Lepidocrocite	48
13	53.7	27	Magnetite	53.7
14	57.22	52	Magnetite	57.2
15	62.78	65	Magnetite	62.7
16	65.16	204	Magnetite	65.1
17	82.44	263	Magnetite	82.3

Table A. 3- XRD peak identification chart for Week 6

IM-1-long -6 weeks				
Peaks	2-Theta	Intensity	Peak identified with	
1	14.28	58	Goethite	14.2
2	18.38	54	Magnetite	18.4
3	21.4	52	Lepidocrocite	21.4
4	23.28	26	Lepidocrocite	23.3
5	25.54	17	Lepidocrocite	25.5
6	27.24	36	Goethite	27.2
7	29.56	134	Goethite	29.6
8	30.26	149	Magnetite	30.2
9	35.62	443	Magnetite	35.6
10	39.58	35	Hematite	39.5
11	43.28	100	Magnetite	43.3
12	44.8	843	Iron- Alpha	44.8
13	48.66	17	Lepidocrocite	48
14	53.56	50	Magnetite	53.5
15	57.1	98	Magnetite	57.2
16	62.84	124	Magnetite	62.8
17	65.12	112	Magnetite	65.1
18	74.12	22	Lepidocrocite	72.1
19	82.38	226	Magnetite	82.3

Table A. 4- XRD peak identification chart for Week 8

IM-1-long -8 weeks				
Peaks	2-Theta	Intensity	Peak identified with	
1	14.26	51	Goethite	14.2
2	18.48	84	Magnetite	18.3
3	21.44	86	Lepidocrocite	21.4
4	27.28	41	Goethite	27.2
5	29.6	198	Goethite	29.6
6	30.26	276	Magnetite	30.2
7	31.78	38	Lepidocrocite	32.1
8	33.42	55	Hematite	33.4
9	35.62	925	Magnetite	35.6
10	36.68	90	Goethite	36.6
11	37.18	82	Magnetite	37.1
12	39.18	43	Hematite	39.6
13	41.42	28	Lepidocrocite	41.5
14	43.3	213	Magnetite	43.3
15	44.8	140	Iron- Alpha	44.8

16	47.7	35	Lepidocrocite	48
17	53.6	85	Magnetite	53.5
18	57.1	227	Magnetite	57.1
19	62.66	293	Magnetite	62.6
20	71.2	33	Magnetite	71.2
21	74.12	62	Lepidocrocite	74.1
22	79.28	24	Magnetite	79.2
23	82.44	41	Lepidocrocite	82.4
24	89.72	83	Magnetite	89.7

6.2 Appendix B

Table B. 1- Microscopic images of cement paste samples

Samples	Sample Photo (no magnification)	Microscopic image of sample
0.4-0		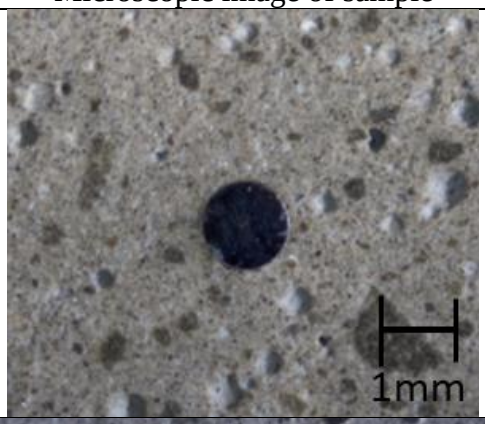
0.35-2		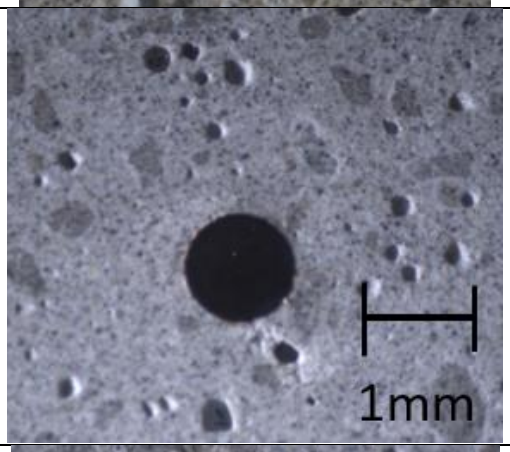
0.35-4		

0.35-6	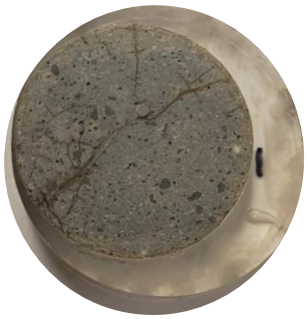	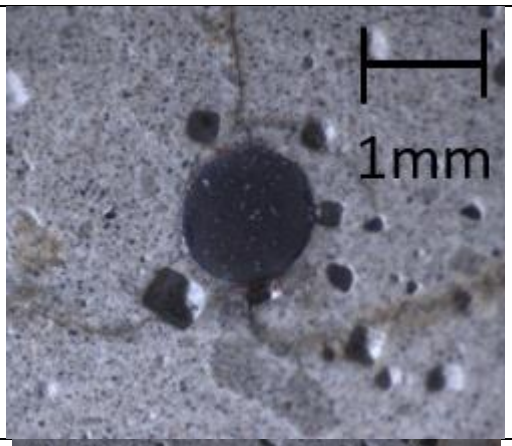
0.35-8		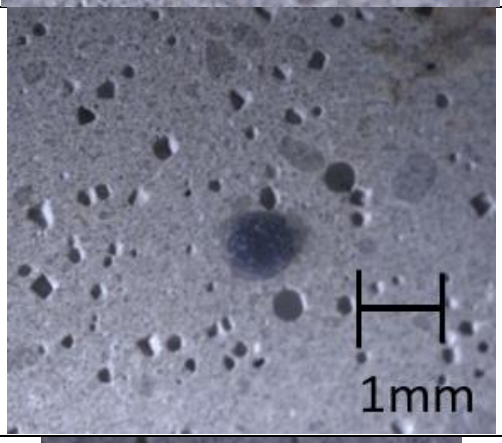
0.4-2		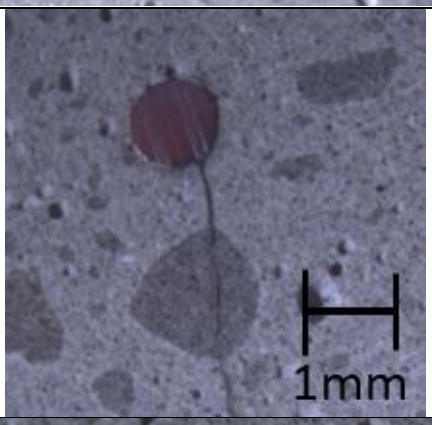
0.4-4		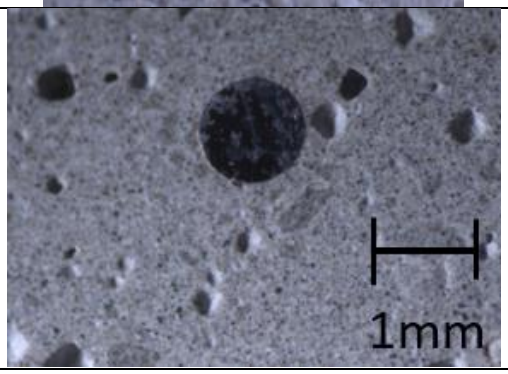

0.4-6	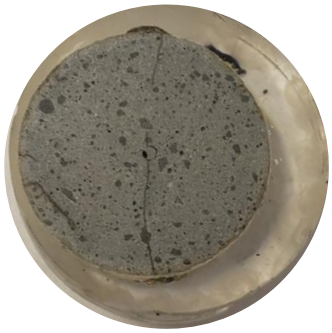	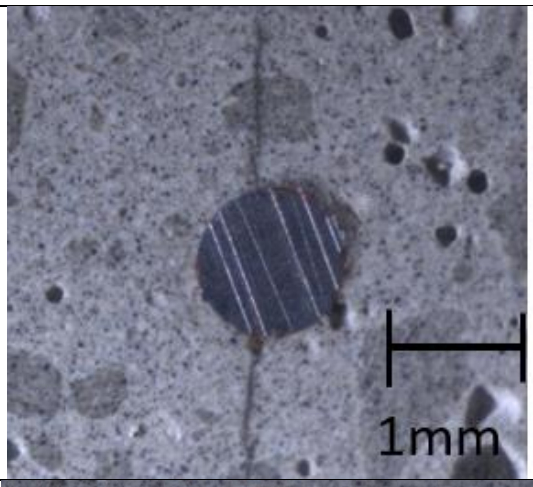
0. 4-8		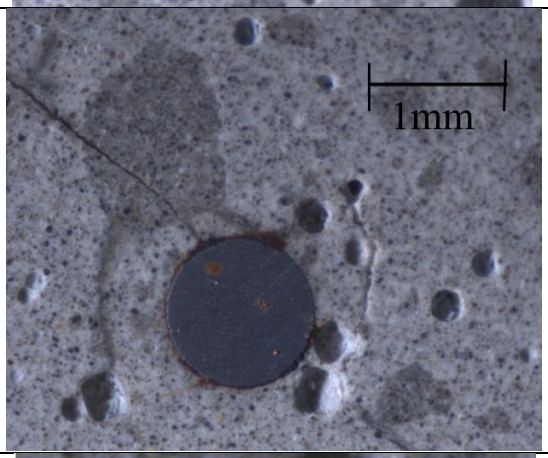
0.5-2		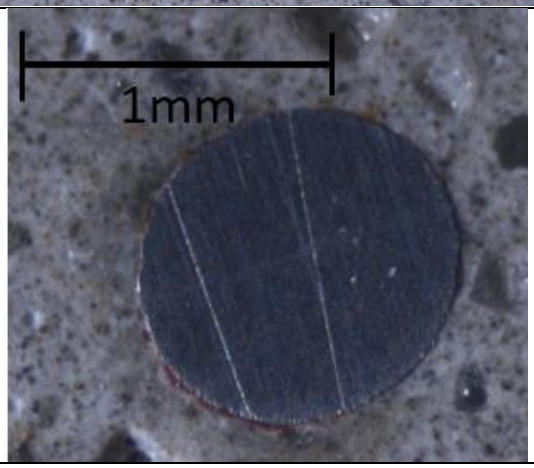

0.5-4		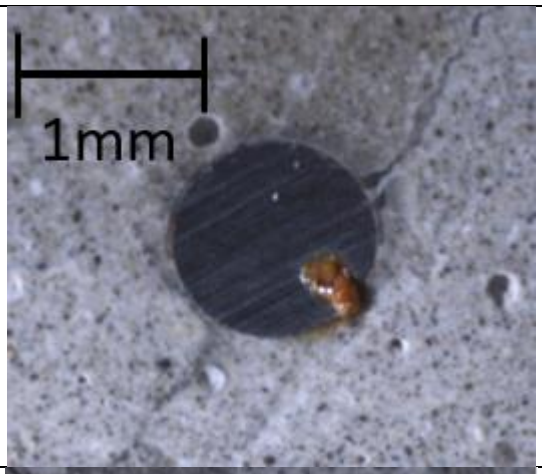
0.5-6		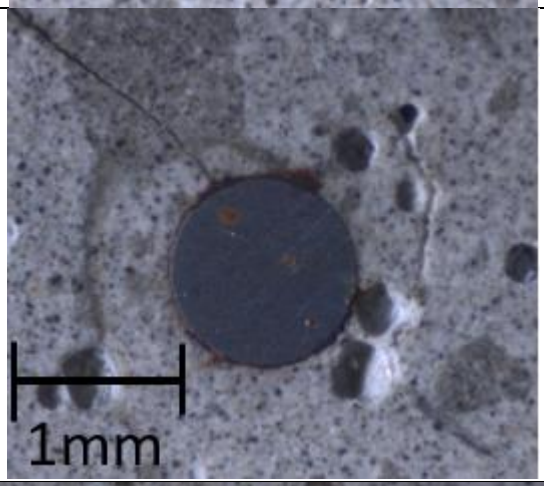
0.5-8		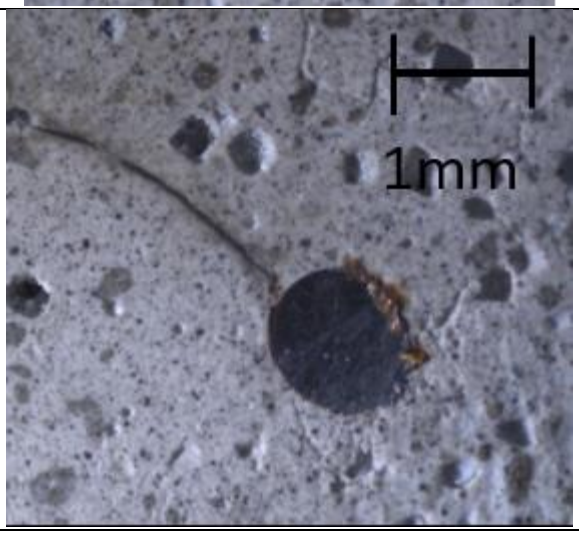

0.4-2(L)		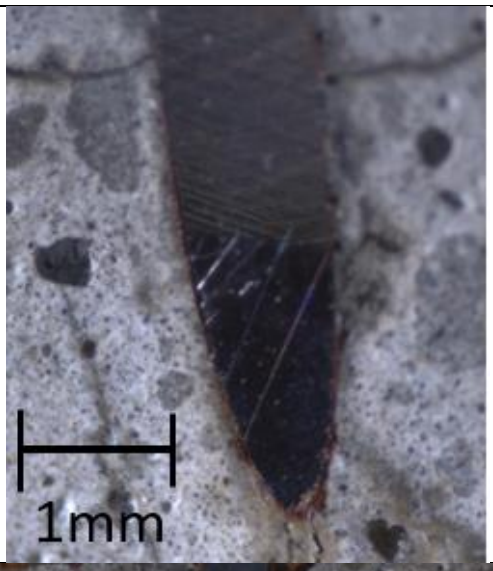
0.4-4(L)		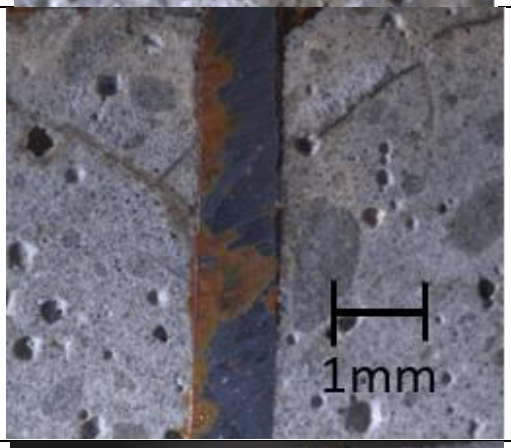
0.4-6(L)		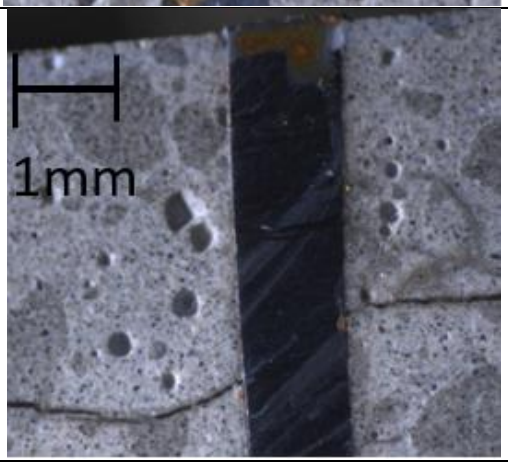

0.4-8(L)		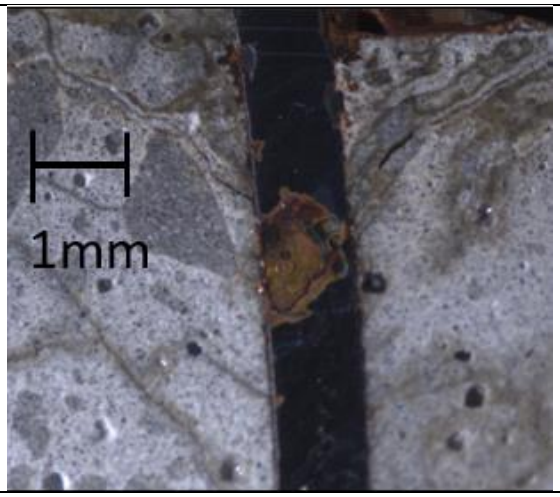

Table B. 2- Description summary of microscopic image

w/c	Duration of accelerated corrosion	Sample #	CP observations	Crack Observations
0.35	2 weeks	0.35-2	• No CP	• No corrosion-induced crack
	4 weeks	0.35-4	• concentrated CP at a specific point •CP is not uniformly distributed around the wire	• 3 corrosion-induced cracks + multiple shrinkage cracks that extend from the outer surface of the cement paste to the wire • Big network of shrinkage cracks
	6 weeks	0.35-6	• CP is not uniformly distributed • More CP at the base of the crack	• 2 corrosion-induced crack • Big network of shrinkage cracks. • The cracks that are closer to the rebar are filled with CP
	8 weeks	0.35-8	• No CP	• No corrosion-induced cracks
0.4	No corrosion	0.4-0	• No CP	• No cracks
	2 weeks	0.4-2	• CP is not uniformly distributed around wire • CP fills the voids around the wire	• 1 corrosion-induced crack 1 • The crack starts at the rebar and extends to the outer surface of the sample. • Only the wider section of the crack is filled with CP
	2 weeks - longitudinal	14	• CP all around the wire • CP is not uniformly distributed • CP seams more concentrated at the bottom of the wire	• 2 corrosion-induced cracks • one crack on each side of the wire and one crack at the bottom end of the wire • the cracks extend from the wire to the outer surface of the cement pate • Small network of thin shrinkage cracks
	4 weeks	0.4-4	• CP covers the whole perimeter of the wire • CP is not uniformly distributed around the wire	• No corrosion-induced cracks
	4 weeks - longitudinal	15	• CP is more concentration on one side of the sample • CP is all over the surface of wire but not uniformly distributed	• No corrosion-induced crack

	6 weeks	0.4-6	• The cracks around the wire are filled with CP • CP is not uniformly distributed around the wire • More CP is found close to pores and cracks	• 2 corrosion-induced cracks • one of the cracks extends from the wire all the way to the outer surface while the other one stops halfway. The third crack originates from the outer surface of the cement paste.
	6 weeks - longitudinal	16	• 1 corrosion-induced crack + multiple shrinkage cracks • small shrinkage cracks are present around the surface perimeter • CP is not uniformly distributed around the wire • More CP is concentrated close to the crack	• 2 corrosion-induced cracks • one crack goes from the wire to the outer surface of the sample • Big network of shrinkage cracks.
	8 weeks	0.4-8	• CP is not uniformly distributed around the wire • Stains of CP are seen on the surface of the wire • More CP is concentrated close to the crack	• 1 corrosion-induced crack + multiple shrinkage cracks • one crack that goes from the wire to the outer surface of the sample • small shrinkage cracks are present around the surface perimeter
	8 weeks - longitudinal	17	• CP concentrated at specific points • more CP at the top and bottom of the wire	• 2corrosion-induced cracks • one crack on each side of the wire and one crack at the bottom end of the wire • the cracks extend from the wire to the outer surface of the cement paste
0.5	2 weeks	0.5-2	• Very little CP • the pores around the wire are filled with CP • CP is not uniformly distributed	• No corrosion-induced crack
	4 weeks	0.5-4	• CP concentrated at a specific point • CP is not uniformly distributed	• 2 corrosion-induced cracks
	6 weeks	0.5-6	• CP is concentrated on one side of the wire	• 1 corrosion-induced crack • One crack extending to the outer surface of the sample • the base of the crack is filled with CP
	8 weeks	0.5-8	• CP is not uniformly distributed • CP fills the void around wire • Some areas around the wire have no visible CP	• 1 corrosion induced crack • the crack extends to the outer surface of the sample